

Disturbed flow increases endothelial inflammation and permeability via a Frizzled-4- β -catenin-dependent pathway

Matthew Rickman², Mean Ghim², Kuin Pang², Ana Cristina von Huelsen Rocha², Elena M. Drudi², Macià Sureda-Vives², Nicolas Ayoub², Virginia Tajadura-Ortega², Sarah J. George³, Peter D. Weinberg², Christina M. Warboys^{1,*}

¹Department of Comparative Biomedical Sciences, Royal Veterinary College, Royal College Street, London, NW1 0TU

²Department of Bioengineering, Imperial College London, London, SW7 2AZ

³Translational Health Sciences, Bristol Medical School, Research Floor Level 7, Bristol Royal Infirmary, Bristol, BS2 8HW, UK

* Author for correspondence:

Dr Christina Warboys

Department of Comparative Biomedical Sciences

Royal Veterinary College, Royal College Street

London, NW1 0TU

cwarboys@rvc.ac.uk

Keywords: mechanotransduction, inflammation, orbital shaker, atherosclerosis, adherens junctions, cytoskeleton,

Summary Statement

Disturbed flow is a key factor in promoting endothelial dysfunction. Frizzled-4 mediates the pro-inflammatory and barrier disrupting effects of disturbed flow in endothelial cells via a WNT5A and β -catenin-dependent mechanism.

Abstract

Multidirectional or disturbed flow promotes endothelial dysfunction and is associated with early atherogenesis. Here we investigated the role of Wnt signalling in flow-mediated endothelial dysfunction. The expression of Frizzled-4 was higher in cultured human aortic

endothelial cells (EC) exposed to disturbed rather than undisturbed flow, obtained using an orbital shaker. Increased expression was also detected in regions of the porcine aortic arch exposed to disturbed flow. The increased Frizzled-4 expression in cultured EC was abrogated following knockdown of R-spondin-3. Disturbed flow also increased the nuclear localisation and activation of β -catenin, an effect that was dependent on Frizzled-4 and R-spondin-3. Inhibition of β -catenin using iCRT5, or knockdown of Frizzled-4 or R-spondin-3, resulted in reduced expression of pro-inflammatory genes in EC exposed to disturbed flow, as did inhibition of WNT5A signalling. Inhibition of the canonical Wnt pathway had no effect. Inhibition of β -catenin also reduced endothelial paracellular permeability; this was associated with altered junctional and focal adhesion organisation and cytoskeletal remodelling. These data suggest the presence of an atypical Frizzled-4- β -catenin pathway that promotes endothelial dysfunction in response to disturbed flow.

List of symbols and abbreviations used

DF	disturbed flow
EC	endothelial cell
eNOS	endothelial nitric oxide synthase
FZD	Frizzled
GSK3β	glycogen synthase kinase-3 β
IL-8	interleukin-8
KLF	Kruppel-like factor
Lrp	lipoprotein-related protein
MCP-1	monocyte chemoattractant protein-1
RSPO	R-spondin
SELE	E-selectin
VCAM	vascular cell adhesion molecule
UF	Undisturbed flow
WSS	wall shear stress
ZO-1	zonula occludens-1

Introduction

Endothelial cells (EC) are continuously exposed to hemodynamic wall shear stress (the frictional force per unit area exerted by flowing blood). Surface mechanosensors enable EC

to sense and respond to this shear stress via various mechanosignalling pathways (Givens, 2016). Regulation of these pathways differs greatly depending on local vessel geometry and the resulting shear stress to which EC are exposed, leading in turn to significant differences in EC function. EC in straight, unbranched regions of arteries experience high magnitude, pulsatile but uniaxial wall shear stress that is a key determinant of EC homeostasis, activating cytoprotective signalling pathways and promoting the expression of KLF-2, KLF-4, eNOS and thrombomodulin. Conversely, EC in atherosclerosis-prone areas within regions of high curvature, branching or bifurcation exhibit endothelial dysfunction, with increased permeability, reduced expression of eNOS and activation of pro-inflammatory signalling pathways (Davies, 2013).

The exact type of shear stress that leads to the latter behaviour is controversial. Recent work has challenged the consensus that low time averaged wall shear stress and a high oscillatory shear index drives EC dysfunction and atherogenesis (Peiffer, 2013) and instead has highlighted the importance of disturbed/multidirectional flow (i.e. high transverse wall shear stress) (Mohamied, 2015); however, the precise trigger is still unknown. The mechanisms by which disturbed flow influences EC behaviour are poorly defined, although some signalling pathways have been identified that contribute to aspects of flow-dependent EC dysfunction (Warboys, 2014; Mahmoud, 2016; Serbanovic-Canic, 2017; Alfaidi, 2020). Our aim is to better understand mechanosignalling and function in endothelial cells exposed to flow that is multidirectional.

The Wnt signalling pathway is known to regulate responses to mechanical forces in non-vascular mechanoresponsive cells (Warboys, 2018) and a similar role in vascular cells is becoming apparent. Non-canonical Wnt ligands regulate EC polarisation in a flow-dependent manner (Franco, 2016) whilst transcriptomic analysis reveals that Wnt pathway genes are significantly enriched in EC exposed to atherogenic flow environments (Maimari, 2016; Bondareva, 2019), suggesting a possible role in promoting flow-mediated EC dysfunction (Bondareva, 2019). Moreover, low/oscillatory shear stress increases β -catenin signalling in endothelial cells, which promotes the activation of NF- κ B (Gelfand, 2011). Wnt signalling pathways (reviewed elsewhere (MacDonald, 2009)) are highly conserved and require the interaction of Wnt with Frizzled receptors on the cell surface. Complexity arises from the presence of multiple Wnt ligands, Frizzled receptors and co-receptors that can

associate in various combinations in a context-dependent manner (Dijksterhuis, 2014). Canonical Wnt signalling requires the dephosphorylation and stabilisation of β -catenin, typically through inhibition of the β -catenin destruction complex, allowing β -catenin to translocate to the nucleus and regulate transcription of target genes via interaction with transcription factors such as TCF-4 (MacDonald, 2009). In this study we sought to investigate and dissect the contribution of canonical Wnt signalling pathways in mediating EC dysfunction in response to disturbed flow using an *in vitro* model that is uniquely capable of creating disturbed/multidirectional flow (Ghim, 2018; Warboys, 2019; Pang, 2021).

Results

Frizzled-4 expression is increased by disturbed flow and promotes endothelial inflammatory signalling

Frizzled-4 (FZD4) mRNA levels were previously shown to be sensitive to flow conditions in a transcriptomic analysis of the porcine aorta (Serbanovic-Canic, 2017). Here we assessed the expression at the protein level following exposure to different flow conditions using the orbital shaker method. Western blot analysis revealed that disturbed flow (DF) significantly increased the expression of Frizzled-4 relative to undisturbed flow (UF) after 24h and that this increase was sustained for 72h of flow exposure (Fig. 1A). Subsequent analysis revealed that DF increases the expression of FZD4 relative to static conditions and UF and that expression levels in EC exposed to static or UF were not significantly different (Fig. 1B). Demonstrating the potential physiological relevance of this finding, we also observed increased FZD4 receptor in the inner curvature of the porcine aortic arch, a region exposed to chronic flow disturbance (Suo, 2007; Serbanovic-Canic, 2017), compared to the outer curvature, a region exposed to undisturbed flow (Fig. 1C).

To determine whether FZD4 mediates endothelial dysfunction under prolonged DF we transfected EC with siRNA targeting FZD4 before exposure to flow. Protein expression of FZD4 was reduced by at least 50% after 48h of flow when compared to EC transfected with scrambled RNA (Fig. S2). The expression of Frizzled-5, Frizzled-6 and Frizzled-7 transcripts were unaffected (Fig. S2). Knockdown of FZD4 resulted in significantly reduced expression of

several flow-dependent pro-inflammatory genes when compared to scrambled transfected controls (*SELE*, *MCP-1*, *VCAM1*; Fig. 1D). This effect was specific to EC exposed to DF. As expected, the expression of pro-inflammatory genes was significantly lower in EC exposed to UF and expression levels were not altered following FZD4 knockdown. We also observed a reduction in VCAM1 protein in EC exposed to DF (Fig. 1E). Knockdown of FZD4 did not alter expression of the flow-sensitive genes KLF-2 and eNOS (Fig. S2), suggesting that EC remain capable of responding to flow.

FZD4 expression under disturbed flow is regulated by R-spondin-3

We next sought to determine the mechanism by which DF elevates FZD4 protein expression. Paradoxically, we found that expression of the FZD4 gene was significantly lower in EC exposed to DF relative to UF (Fig. 2A), pointing towards a post-transcriptional or post-translational mechanism. Since FZD4 protein expression can be regulated by lysosomal degradation, mediated by RNF/ZNRF3 ubiquitin ligases (Koo, 2012; Hao, 2016), we explored the regulation of this pathway by flow. We found no observable difference between the expression levels of ZNRF3 under DF and UF (Fig. 2B) but we did observe a significant increase in the expression of R-spondin 3 (RSPO-3), which inhibits ZNRF3 (Hao, 2012), in EC exposed to DF at both the gene (Fig. 2C) and protein level (Fig. 2D). The expression of RSPO-1 -2 and -4 was undetectable in these cells. These data are consistent with the DF-dependent increase in FZD4 being caused by an increased expression of RSPO-3, which would inhibit its degradation. Supporting this view, FZD4 protein expression was significantly reduced in EC under DF conditions following knockdown of RSPO-3 (Fig. 2E-F). Moreover, knockdown of RSPO-3 also reduced the expression of *SELE* and *VCAM1* in EC exposed to DF (Fig. 2G), mirroring the effects of FZD4 knockdown.

These data suggest that DF induces pro-inflammatory changes by increasing the expression of FZD4. Subsequent studies focused on understanding the pathways by which FZD4 determines these and other changes in EC exposed to DF.

FZD4 signalling in EC exposed to disturbed flow is mediated by increased transcriptional activity of β -catenin

FZD4 is known to activate the canonical, β -catenin-dependent Wnt pathway. Previous studies have also determined that β -catenin can be activated in response to low/oscillatory or atherogenic shear stress (Gelfand, 2011; Li, 2014) but it is not clear whether multidirectional flow (DF) has the same effects. We therefore examined whether the anti-inflammatory effects of FZD4 knockdown under DF conditions were associated with altered β -catenin signalling. Analysis of fractionated lysates revealed that total β -catenin expression was significantly increased in both cytosolic and nuclear fractions of EC exposed to DF compared to those exposed to UF, similar to results reported for low and/or oscillatory shear stress (Gelfand, 2011; Li, 2014). Nuclear expression of the active, dephosphorylated form of β -catenin was also significantly increased in EC exposed to DF (Fig. S3). Using a reporter assay we demonstrated that DF (1h – 48h) significantly increased reporter activity relative to UF, indicating increased β -catenin-mediated transcriptional activity. Reporter activity in EC exposed to DF also increased over time (Fig. S3). These data support the findings of previous studies that atherogenic flow conditions activate β -catenin signalling (Gelfand, 2011; Li, 2014).

Previous studies have also shown that β -catenin can activate inflammatory pathways under atherogenic shear stress (Gelfand, 2011). We sought to confirm these findings in EC exposed to DF using iCRT5, a small molecule inhibitor of β -catenin transcriptional activity (Gonsalves, 2011). Addition of iCRT5 to EC for the last 24h of flow exposure significantly inhibited β -catenin transcriptional activity (Fig. 3A) and reduced the expression of *SELE*, *MCP-1* and *VCAM1* transcripts specifically under DF conditions relative to vehicle-treated controls (Fig. 3B). The addition of iCRT5 had no effect on pro-inflammatory gene expression in EC exposed to UF (Fig. 3B). Similar results were obtained when iCRT5 was added for the duration of flow or when β -catenin expression was reduced following transfection of EC with siRNA targeting β -catenin (Fig. S4). Treatment with iCRT5 for the final 24h of flow exposure also significantly attenuated the up-regulation of pro-inflammatory genes induced by $\text{TNF}\alpha$ (Fig. 3C). Furthermore, addition of iCRT5 for the final 24h of flow exposure resulted in significantly reduced adhesion of monocytes to EC exposed to DF (Fig. 3D). Similar results were obtained when iCRT5 was added for the duration of flow (data not shown). These data support the

idea that β -catenin modulates inflammatory activation in response to atheroprone flow and they mirror the effects of FZD4/RSPO-3 knockdown.

Importantly, reduction of FZD4 expression by siRNA interference resulted in a significant decrease in β -catenin transcriptional activity under DF conditions. No effect was observed in EC exposed to UF (Fig. 3E). FZD4 knockdown was also associated with reduced β -catenin protein levels in whole cell lysates (Fig. 3F). Transcript levels of β -catenin were unaffected (Fig. 3G). Moreover, knockdown of RSPO-3 also reduced the expression of β -catenin in whole cell lysates under DF conditions (Fig. 3F). These data suggest that FZD4-dependent activation of β -catenin mediates, at least in part, the pro-inflammatory effects of DF.

Inhibition of WNT5A signalling reduces disturbed flow-dependent activation of β -catenin and attenuates inflammatory signalling

Since Frizzled receptors are commonly activated by Wnt ligands, we assessed the role of WNT5A in mediating the response to DF. We focused on WNT5A because it is known to promote inflammatory signalling in EC (Bretón-Romero, 2016). We found significantly increased expression of WNT5A in EC exposed to DF compared to UF at both the transcript (Fig. 4A) and protein level (Fig. 4B). Transfection with WNT5A siRNA resulted in a 35-40% reduction in WNT5A expression (Fig. 4C) and reduced expression of *SELE*, *MCP-1* and *VCAM1* (Fig. 4D).

These data suggest that WNT5A can promote endothelial dysfunction under DF conditions. This interpretation was supported by experiments where EC were treated with SFRP-1, which blocks the interaction of WNT5A with Frizzled receptors (Dufourcq, 2008) and is shown here to reduce β -catenin reporter activity (Fig. 4E). Similar to knockdown of WNT5A and FZD4 and inhibition of β -catenin signalling, SFRP-1 treatment for 24h significantly reduced the expression of *SELE* and *MCP-1* in EC exposed to DF (Fig. S6). Interestingly, inhibition was greater when cells were exposed to SFRP1 for 72h and the expression of *VCAM1* was also significantly reduced (Fig. 4F).

FZD4 signalling in EC exposed to disturbed flow acts via GSK3 β but is independent of LRP5/6

The data presented so far suggests that EC dysfunction under DF conditions can be promoted via WNT5A-FZD4 signalling. The requirement for β -catenin is consistent with the involvement of a canonical (β -catenin-dependent) Wnt signalling pathway, and this is supported by the finding that phosphorylation of GSK3 β (Ser9) was increased in EC by exposure to DF compared to UF (Fig. 5A). Phosphorylation of the Ser9 residue inhibits GSK3 β and is a necessary step in the activation of β -catenin; it results in inhibition of the β -catenin destruction complex leading to the nuclear localisation of dephosphorylated (active) β -catenin. GSK3 β phosphorylation on Ser9 was significantly reduced following knockdown of FZD4 or RSPO-3 (Fig. 5B) suggesting a role for the destruction complex in mediating their effects on β -catenin signalling in EC exposed to DF. We consequently investigated whether stabilisation of the β -catenin destruction complex affected the activation of β -catenin and the phenotype of EC exposed to DF. We found that treating the cells with IWR-1 (which stabilises Axin2 levels) inhibited the transcriptional activity of β -catenin and reduced the expression of *SELE* and *MCP-1* under DF conditions, mimicking the effects of WNT5A and FZD4 knockdown and inhibition of β -catenin signalling (Fig. 5C-D). These data are consistent with a role for activation of a FZD4-dependent canonical Wnt pathway in cells exposed to DF.

To test this further, we assessed the activation of LRP6 (a hallmark of the canonical Wnt pathway) under flow conditions. Surprisingly, we found no evidence of greater LRP6 phosphorylation under DF than under UF (Fig. 5E). Total levels of LRP6 protein were also unchanged (Fig. 5F). Moreover, inhibiting canonical Wnt signalling by treating EC with DKK-1 (which blocks the interaction of LRP and Frizzled receptors) for 24h did not have the expected effect on the expression of proinflammatory genes (Fig. 5G) or THP-1 monocyte adhesion (data not shown). A similar lack of effects was observed when DKK-1 was added for the duration of flow exposure (data not shown).

Because these data suggest that FZD4 activates β -catenin independently of LRP signalling, we investigated alternative Wnt pathway components that could mediate the effects of FZD4 activation and found that Ryk expression was significantly increased in EC exposed to DF for 72h (Fig. 5H). Transfection with Ryk siRNA resulted in a significant reduction in Ryk

expression (Fig. 5I) and was associated with reduced levels of β -catenin in EC exposed to DF (Fig. 5J), consistent with a role in regulating β -catenin under DF conditions. Moreover, knockdown of Ryk reduced the expression of *VCAM1* in cells exposed to DF (Fig. 5K).

Inhibiting β -catenin activity reduces the elevated paracellular permeability seen in monolayers exposed to disturbed flow

Aside from increased pro-inflammatory signalling, DF-induced endothelial dysfunction is also associated with increased endothelial permeability (Wu, 2015; Ghim, 2017; Lyu, 2019; Alfaidi, 2020; Yang, 2020). DF increases monolayer permeability to FITC-avidin compared to UF or static culture by a paracellular route (Ghim, 2017, 2022). Since inhibition of β -catenin signalling altered DF-induced inflammatory activation, we assessed whether inhibition could also alter barrier function in EC exposed to DF. Inhibition of β -catenin transcriptional activity using iCRT5 significantly reduced permeability to FITC-avidin under DF (Figs. 6A and 6B). Permeability of EC exposed to UF was not affected (Fig. 6B). Closer inspection showed that transport at bicellular junctions appeared to be particularly reduced (Fig. S5). Immunostaining of ZO-1 and VE-cadherin revealed a clear change in junctional organisation following inhibition of β -catenin in EC exposed to DF, along with increased expression of ZO-1 (Fig. 6C and quantified in Fig. S5). Junctions appeared disorganised and irregular in control EC exposed to DF but more organised following treatment with iCRT5 (Fig. 6C). The morphology of EC exposed to DF was also altered by iCRT5: the cells appeared more consistently oriented and more elongated (representative images in Fig. 6C-E). Quantification of the length-to-width ratio confirmed the latter observation (Fig. S5; UF included for reference).

We also assessed the effects of β -catenin inhibition on the actin cytoskeleton in cells exposed to DF. Staining with phalloidin revealed striking differences after treatment with iCRT5. There was a reduction in the number of stress fibres and an increase in junctional (cortical) staining that is typically associated with stabilisation of junctions and reduced permeability (Fig. 6D) (McCue, 2004). The distribution of vinculin under DF was also modified by iCRT5: there was greater localisation around junctions compared to the apparent localisation to focal adhesions in untreated cells (Fig. 6E). There was a similar

change in morphology, junctional organisation, cytoskeletal architecture and vinculin localisation following knockdown of FZD4 (Fig. 7A-C).

Knockdown of WNT5A also resulted in reduced numbers of stress fibres, increased cortical actin, and apparent elongation of EC exposed to DF, similar to the effects observed with knockdown of FZD4 or inhibition of β -catenin signalling with iCRT5 (Fig. 7D). Furthermore, SFRP-1 and IWR-1 treatment also resulted in morphological, junctional and cytoskeletal changes similar to those observed previously (Fig. S6 and Fig. S7). DKK-1 had no effect on length-to-width ratio or cytoskeletal/junctional organisation (Fig. S5 and Fig. S7).

Increased permeability can be associated with EC undergoing endothelial-mesenchymal transition (End-MT) and this process is known to be increased by DF (Mahmoud, 2017) and by canonical Wnt signalling (Liebner, 2004). No evidence was found here to suggest that this was a contributing factor since iCRT5 or FZD4 knockdown had no effect on the expression of genes associated with End-MT (see Fig. S5). We subsequently investigated whether inhibiting β -catenin signalling affected the expression of junctional molecules. iCRT5 did not induce changes in the transcript levels of *VE-CADHERIN*, *ESAM*, *JAM-B* or *CTNNB1* in EC exposed to DF. However, it did increase expression of *PECAM-1*, *JAM-A*, *JAM-C*, *ZO-1* and *CLDN-5* (Fig. 7E). Taken together these data suggest that inhibiting β -catenin signalling increases the expression of junctional proteins and stabilises cell-cell junctions in EC exposed to DF and that this may account for the enhanced barrier properties observed in the presence of iCRT5.

Discussion

Here we provide evidence of a novel FZD4-dependent signalling pathway, summarised in Fig. 8, that is activated in EC in response to disturbed flow (DF). The expression of FZD4 is significantly higher under DF than undisturbed flow (UF), and that is dependent on increased expression of RSPO-3. In response to DF, FZD4 increases the transcriptional activation of β -catenin independently of LRP signalling. β -catenin promotes the inflammatory activation and barrier disruption associated with DF.

The expression of FZD4 in the developed arterial circulation has been demonstrated previously (Descamps, 2012) but to our knowledge this is the first evidence that FZD4 protein expression is elevated in response to DF. FZD4 transcript levels decreased under the same conditions. This observation is in line with data obtained following surgical induction of flow disturbance in mouse carotid arteries (Ni, 2010), but a second transcriptomic analysis found *increased* FZD4 transcript levels in the inner curvature of the porcine aortic arch; this may reflect an adaptation to chronic DF exposure (Serbanovic-Canic, 2017). Regardless of the apparent discrepancies in transcript levels between earlier studies, we found increased FZD4 protein in the inner curvature of the porcine aortic arch, which is chronically exposed to DF, suggesting that the increased protein expression in our cell culture model is physiologically relevant.

We show here that FZD4 contributes to the proinflammatory activation of EC under DF. Interestingly, FZD4 is also required for retinal vascular development and regulates arterial organisation in response to hindlimb ischaemia (Descamps, 2012). In these experiments FZD4 was shown to increase proliferation and migration although these studies were carried out under static conditions (Descamps, 2012). FZD4 function therefore appears to be context and stimulus dependent – whilst it can play a homeostatic role it also appears to promote endothelial dysfunction in EC exposed to DF.

Since FZD4 protein levels were elevated under DF without any concomitant rise in transcript levels, we investigated other mechanisms of regulation. E3 ubiquitin ligases ZNRF3 and RNF43 target Frizzled for lysosomal degradation and thus negatively regulate Frizzled signalling (Hao, 2012). We did not observe any change in expression of these enzymes under flow conditions. However, we did find a significant increase in the expression of RSPO-3, which inhibits the activity of ZNRF3 (Hao, 2012), in EC exposed to DF. This plausibly explains the increase in FZD4. Knockdown of RSPO-3 significantly lowered the expression of FZD4 in cells exposed to DF and reduced the inflammatory activation induced by this type of flow, further supporting a role for RSPO-3 in the regulation of FZD4 under DF. The mechanism by which RSPO-3 is increased by DF is not currently known and will be an important area for future study.

Whilst we have shown that reducing FZD4 attenuates DF-induced inflammatory activation, the mechanisms by which FZD4 signalling is activated are not fully defined. One possibility is that, as a G-protein coupled receptor, FZD4 may be directly activated by mechanical force, as has been demonstrated for other GCPRs (Hu, 2021). FZD4 may also require ligand binding as has been demonstrated in bone mesenchymal stem cells, where WNT5A is required for the activation of FZD4 in response to mechanical forces (Gu, 2018). Interestingly, deletion of WNT5A increases the sensitivity of EC to laminar shear stress, lowering the threshold at which EC polarise against flow direction (Franco, 2016), although its role in regulating responses to non-uniform shear stress had not previously been explored.

Our data support a role for WNT5A in mediating DF-induced inflammatory activation: the expression of WNT5A was increased in EC exposed to DF and knockdown of WNT5A reduced the expression of proinflammatory genes under DF. The mechanism by which WNT5A expression is increased by disturbed flow was not determined and is an area of future study. Further evidence for the importance of ligand-mediated activation of FZD4 is provided by data showing that DF-induced activation of β -catenin and proinflammatory signalling is also reduced following treatment with SFRP-1, which binds and antagonises FZD4 (Dufourcq, 2008), although it should be noted that SFRP-1 may have actions at other Frizzled receptors (Dufourcq, 2008; Pereira, 2008). Our data support the finding that WNT5A promotes canonical Wnt signalling when FZD4 expression is high (Mikels, 2006).

WNT5A has previously been shown to promote endothelial dysfunction in static EC (Bretón-Romero, 2016; Cho, 2018) via a JNK-dependent pathway (Bretón-Romero, 2016). We found no evidence of JNK activation in cells exposed to DF (see Fig. S8), suggesting that non-canonical WNT5A-JNK signalling is not important in mediating responses to DF. Our data instead support a role for a canonical Wnt pathway since knockdown of FZD4 and RSPO-3 reduced the activation of β -catenin in EC exposed to DF. Our observation of increased GSK3 β under DF also indicates the presence of a flow-sensitive canonical pathway. However, we could not detect the phosphorylation of LRP6 that is typically associated with canonical Wnt signalling. Furthermore, inhibition of the canonical pathway using DKK-1 (which blocks the interaction between Frizzled and LRP co-receptors) had no effect on EC responses to DF. It is possible that upon stimulation, FZD4 directly activates the β -catenin destruction complex, independently of LRP5/6. This could occur as a result of dimerization

of FZD4 receptors and consequent clustering of Dishevelled (DVL) proteins (Gammons, 2016), leading to the dimerization and polymerisation that is necessary for activation of the axin degradasome (Gammons, 2018). Alternatively, WNT5A-FZD4 signalling may occur independently of DVL, as has been demonstrated during neurite outgrowth (Bian, 2015).

Intriguingly, it has also been documented that WNT5A can promote endothelial dysfunction via the Wnt co-receptor, Ryk, an atypical receptor kinase that lacks kinase activity (Skaria, 2017). Ryk can associate with Frizzled receptors and DVL in 293T cells and this is required for transcriptional activity of TCF4 (Lu, 2004). However, a direct interaction with Wnt pathway components has not previously been demonstrated in EC. We demonstrated here that Ryk expression is increased in EC exposed to DF and that depletion of Ryk reduces GSK3 β phosphorylation and VCAM1 expression under DF. It is therefore possible that Ryk is recruited to FZD4 receptors upon ligation by WNT5A and contributes to the activation of β -catenin. Taken together, our data suggest the presence of an atypical Wnt signalling pathway that is activated by DF and promotes endothelial dysfunction. Interestingly, Gelfand et al. also provide evidence that PECAM-1 plays a role in the regulation of β -catenin under atherogenic flow conditions (Gelfand, 2011) and that this could be due to phosphorylation and consequent inhibition of GSK3 β (Biswas, 2006); DF-induced activation of β -catenin is thus complex and may require multiple converging pathways.

We have shown here that the increased expression of RSPO-3 and FZD4 in EC exposed to DF results in increased nuclear translocation and transcriptional activation of β -catenin. Similar findings were previously obtained in EC exposed to low and oscillatory shear stress for 6-24h (Gelfand, 2011; Li, 2014), suggesting that activation of β -catenin is common under atherogenic flow conditions. We also demonstrated that increased transcriptional activity of β -catenin resulted in increased expression of pro-inflammatory molecules (*VCAM1*, *MCP-1*, *SELE*) and increased adhesion of THP-1 monocytes in EC exposed to DF. Interestingly, RSPO-3 has also been shown to enhance non-canonical Wnt/Ca²⁺/NFAT signalling in endothelial cells (Scholz, 2016). The regulation of non-canonical pathways by FZD4 under flow conditions is an important area for future research.

In addition to its actions on proinflammatory signalling, our data reveal important effects of flow-activated Wnt signalling and β -catenin transcriptional activity on cell morphology, cytoskeletal organisation and permeability. Ghim et al. recently demonstrated that

monolayers exposed to DF exhibit increased permeability to FITC-avidin, which we confirmed here (Ghim, 2017, 2022). We additionally found that inhibiting β -catenin transcriptional activity with a small molecule inhibitor significantly reduced endothelial permeability. It is likely that these effects are specific to arterial EC since there appear to be key differences in Wnt- β -catenin signalling between the systemic circulation and the blood-brain/blood-retinal barrier. β -catenin plays a critical role in the development of the blood-brain barrier but appears to have little effect on embryonic vascular development in other arterial beds (Cattelino, 2003; Daneman, 2009). Moreover, conditional endothelial deletion of β -catenin impairs the integrity of the blood brain barrier whereas it has no effect on the integrity of the pulmonary vasculature (Tran, 2016).

EC exposed to DF exhibited a randomly oriented cobblestone morphology and a disorganised actin cytoskeleton with numerous stress fibres. Immunostaining for ZO-1, PECAM-1 and VE-cadherin revealed irregular and disorganised junctions, in line with other observations (Alfaidi, 2020). Inhibition of the flow-dependent Wnt pathway at various levels appeared to promote the formation of more organised junctions, plausibly accounting for the reduction in permeability it caused. We also observed a significant increase in *JAM-A*, *JAM-C*, *Claudin-5* and *ZO-1* transcript levels following inhibition of β -catenin transcriptional activity. A role for ZO-1 in maintaining VE-cadherin function has been seen in EC cultured under static conditions: ZO-1 increases tensile force on VE-cadherin, promotes the formation of cortical actomyosin structures and recruits vinculin to adherens junctions (Tornavaca, 2015). We also demonstrated in this study that blockade of the DF-induced Wnt pathway is associated with redistribution of vinculin to cell-cell contacts. This is consistent with other evidence suggesting that vinculin binds to VE-cadherin and stabilises adherens junctions during force-dependent remodelling (Huvneers, 2012).

Blockade of the Wnt pathway and β -catenin transcriptional activity was also associated with EC elongation and alignment, accompanied by the formation of the dense cortical actin ring typically observed in EC exposed to unidirectional shear stress (Birukov, 2002; McCue, 2004) and associated with enhanced barrier function (Garcia, 2001). Recent studies provide evidence that EC re-orient and align themselves so as to minimise transverse wall shear stress (Arshad, 2021) and that EC fail to remodel when transverse wall shear stress is high, resulting in inflammatory activation (Wang, 2012) and increased permeability (Ghim, 2017).

It is known that unidirectional shear stress induces cytoskeletal remodelling and consequent permeability reduction via rapid activation and translocation of Rac and cortactin to cell-cell junctions (Birukov, 2002), along with paxillin and FAK (Shikata, 2003). However, the mechanisms governing permeability and cytoskeletal organisation under disturbed flow are less well defined although there appears to be a requirement for activation of p21-activated kinase (PAK) (Alfaidi, 2020). Here we report that following inhibition of the flow-dependent Wnt pathway at various levels, EC appear to undergo dramatic remodelling of junctions and the cytoskeleton even though transverse wall shear stress remains high. Several Wnt pathway components can interact with and regulate the cytoskeleton (Lai, 2009), but our data point towards transcriptional regulation of cytoskeletal components e.g. ZO-1 or other unidentified effectors. It is also possible that blocking FZD4/ β -catenin signalling interferes with a directional flow sensor so that cells are less able to respond to DF. We observed similar alterations to EC morphology under DF following treatment with resveratrol (Warboys, 2014). Future studies should investigate whether inhibition of β -catenin signalling can switch cells exposed to atherogenic DF to an atheroprotective phenotype.

Our finding that β -catenin-dependent transcriptional activity alters cytoskeletal organisation in response to DF via WNT5A-FZD4 signalling is supported by a previous study of human coronary artery EC cultured under static conditions. Here, gene expression profiling revealed enrichment of genes involved in cytoskeletal remodelling following exposure to WNT5A, which was associated with increased endothelial permeability (Skaria, 2017). The effects of WNT5A were mediated by Ryk (Skaria, 2017), which is consistent with our data showing a potential role for Ryk in mediating responses to DF. Although the authors did not explore whether FZD4 and β -catenin were involved, a subsequent study found that RSPO-3 was also associated with barrier disruption in EC cultured under static conditions; in this case, downstream mechanisms were not studied (Skaria, 2018). Conversely, WNT5A has also been shown to stabilise the interaction of vinculin with adherens junctions and strengthen cell-cell interactions (Carvalho, 2019), although these experiments were performed in static EC and WNT5A exerted its effects via Ror2, further demonstrating that Wnt-Frizzled signaling is highly context dependent. We speculate that under DF, elevated RSPO-3 and WNT5A act synergistically to increase signalling through FZD4 and Ryk, leading to increased transcriptional activity of β -catenin and expression of genes that promote the

formation of stress fibres, disorganisation of adherens junctions, increased permeability and endothelial dysfunction.

In conclusion, our results demonstrate that inhibition or deletion of β -catenin reduces inflammatory signalling and enhances barrier function thus pointing towards a role for β -catenin in disturbed flow-induced endothelial dysfunction. However, our previous research demonstrates that β -catenin can also play a pro-survival role in EC exposed to disturbed flow (Tajadura, 2020). We have also shown that β -catenin can interact with eNOS in EC (Warboys, 2014) and that β -catenin is required for maximal activation of eNOS in EC exposed to UF (Tajadura, 2020). The functions of β -catenin under flow conditions are thus complex. Further research is required to understand the dual functions of β -catenin signalling in EC, and further understanding of upstream and downstream pathways is necessary before such signalling can form the basis of therapeutic interventions.

Materials and Methods

Culture of human aortic endothelial cells and exposure to flow

Human aortic endothelial cells (HAEC) from male and female donors were obtained from Promocell and cultured on fibronectin-coated plasticware in Promocell Endothelial Growth Medium MV with Supplement Mix. Culture medium was replaced every 48-72h and cells were sub-cultured using Trypsin-EDTA solution (0.25%). For flow experiments, cells were seeded at passage 7 in 6-well plates coated with fibronectin ($10\mu\text{g}\cdot\text{ml}^{-1}$) and cultured for 24-48h until confluent. For immunostaining experiments, cells were seeded in glass-bottomed 6-well plates (Cellvis). Once confluent, 1.902 ml fresh medium was added to each well (equivalent to 2mm medium height). Plates were placed on an orbital shaker housed inside the incubator (Grant Instruments; 150rpm with 5mm orbital radius) and exposed to flow, induced by the swirling of the medium across the base of the well (Ghim, 2017; Warboys, 2019). Previous computational fluid dynamics studies have shown that EC in the central region of the well (0-7 mm radial distance from the centre of the well) experience low magnitude (<0.3 Pa) multidirectional flow (disturbed flow; DF) whereas EC in the peripheral region of the well (10-16 mm radial distance from the centre of the well) experience high magnitude (>0.5 Pa) unidirectional flow (undisturbed flow; UF) (Ghim, 2018; Pang, 2021)

(see also Fig. S1). The mechanobiology of EC exposed to flow using the method has been well characterised with EC in the centre of the well exhibiting endothelial dysfunction (Warboys, 2019).

In some experiments, cells were treated with the following inhibitors: iCRT5 (50 μM ; Abcam), huDKK-1 (250 $\text{ng}\cdot\text{ml}^{-1}$; R&D Systems) or huSFRP-1 (100 $\text{ng}\cdot\text{ml}^{-1}$; Peprotech). Inhibitors were added for the duration of flow exposure (72h) or for the last 24h of flow exposure (24h) as indicated below. DMSO (0.1% v/v), PBS (0.25% v/v) or H₂O (0.2% v/v) was used as a vehicle control, respectively. Additional details are included in Table S1.

Computational fluid dynamics

Flow simulations were carried out with Star CCM+ (version 11.02.009, CD-Adapco, USA). A single well of a 6-well plate was represented as a cylinder with height of 10 mm and radius of 17.4 mm. The geometry was discretized using a structured cylindrical mesh with 360,000 grid elements. The explicit unsteady model was used. A no-slip condition was imposed at all walls and surface tension was neglected. The top surface of the cylinder was defined as a pressure outlet. The dynamic viscosity and density of medium were $0.78 \times 10^3 \text{ Pa}\cdot\text{s}$ and $1003 \text{ kg}/\text{m}^3$ respectively. The rotation of the well was modelled by introducing a translating gravitational force with the form

$$[x, y, z] = [A\omega^2\cos(\omega t), A\omega^2\sin(\omega t), -9.81]$$

where A is the orbital radius of the shaker, ω is the angular velocity and t is time. The Volume of Fluid model was used to track the free surface of the liquid, which had a height of 2 mm when the well was stationary. Time steps of $1 \times 10^{-4} \text{ s}$ were each iterated 5 times. Maximum WSS at the base of the well was used to assess convergence. A mesh independence study was performed using 720,000 grid elements, and no difference was observed.

Transfection with siRNA and TCF reporter plasmid

Prior to seeding into fibronectin-coated 6-well plates, EC were transfected with 100 nM MISSION® predesigned validated siRNA (see Table S1) or scrambled siRNA control or Cignal™ reporter plasmid (500 ng). Transfection was carried out by electroporation using a Neon™ Transfection System according to the manufacturer's instructions. Electroporated cells were seeded directly into wells containing Endothelial Growth Medium (approx. 5×10^5 cells per well) and cultured for 6-8 h until firmly adhered and confluent. Culture medium was replaced before exposure to flow (as above). For transfection experiments, EC were exposed to flow for 48h to ensure knockdown efficiency.

Luciferase Reporter Assay

Using a template, EC were scraped and aspirated from wells to leave only the DF or UF region, defined above. After scraping, the remaining cells were lysed with Passive Lysis Buffer (Promega) for 15 min at room temperature with constant agitation. Lysates were collected and vortexed briefly. TCF/LEF reporter activity was assessed using a Dual-Luciferase® Reporter Assay System (Promega) according to the manufacturer's instructions. Luminescence of Firefly and *Renilla* luciferase reporters was quantified using a Varioskan Flash Plate Reader. The activity of the Firefly (experimental) reporter was normalised to the activity of the *Renilla* (control) reporter to account for differences in transfection efficiency. Normalised values were also corrected for protein concentration to account for any variations in cell lysis.

Monocyte adhesion assays

THP-1 monocytes (ATCC®) were cultured in suspension in RPMI-1640 medium supplemented with FBS (10%), L-glutamine (2 mM), Penicillin-Streptomycin (100 IU.ml^{-1}) and β -mercaptoethanol (50 μM). Culture medium was replaced every 48-7h and cell density maintained at $8 \times 10^5 - 1 \times 10^6 \text{ cells.ml}^{-1}$. Prior to adhesion assays, THP-1 monocytes were incubated with Calcein-AM ($1 \mu\text{g.ml}^{-1}$) for 20 min at 37°C. Following labelling, monocytes were washed, re-suspended in EC growth medium and added to endothelial monolayers that had been exposed to flow for 72h in the presence or absence of iCRT5. In a subset of experiments, EC were pre-treated with TNF α (10ng/ml) for the final 24h of flow exposure. THP-1 monocytes (1×10^6 per well) were incubated with EC monolayers at 37°C under static

conditions for 60 min. Unbound monocytes were removed by extensive washing and adherent cells fixed using paraformaldehyde (4%) for 5 min. Images of adherent monocytes were acquired with a Zeiss Axioplan epifluorescence microscope using a 20× objective with 470/40 nm excitation and 525/50 nm emission filters. The total number of adherent monocytes was captured across 5 fields of view from the centre of each well.

RNA isolation and qRT-PCR

Using a template, EC were scraped and aspirated from wells to leave only the DF or UF region (as above), from which RNA was obtained by addition of RLT lysis buffer (QIAGEN). In order to obtain enough material, cells from DF or UF regions from 3 wells were pooled. RNA was isolated using RNeasy Mini Kits with on-column DNase digestion (Qiagen) according to the manufacturer's instructions. A High-Capacity Reverse Transcription Kit (Thermo Fisher) was used to prepare cDNA according to the manufacturer's instructions. Transcript levels were assessed by quantitative real-time PCR (Applied Biosystems StepOnePlus™ Real-Time PCR System) using Fast SYBR Green MasterMix (ABI) and gene-specific primers (see Table S2). Reactions were carried out using an Applied Biosystems StepOnePlus™ Real-Time PCR System as follows: 95°C for 20 sec, followed by 40 cycles of 95°C for 3 sec and 60°C for 30 sec. All reactions were performed in triplicate and relative expression assessed by the $\Delta\Delta C_t$ method, using GAPDH as a reference gene.

Protein extraction and western blotting

Using a template, EC were scraped and aspirated from wells to leave only the DF or UF region (as above), from which protein lysates were obtained by addition of RIPA buffer (SDS (0.1%), Triton-X 100 (1%), sodium deoxycholate (0.5%), NaCl (150 mmol/l), Tris (50mmol/l) at pH 7.4) supplemented with protease and phosphatase inhibitor cocktails (Sigma). In order to obtain enough material, cells from DF or UF regions from 3 wells were pooled. Lysates were incubated on ice for 45 min with regular vortexing and centrifuged at 12,000 rpm for 10min to separate soluble and insoluble fractions. For analysis of cytosolic and nuclear fractions, cells were lysed using NE-PER™ Nuclear and Cytoplasmic Extraction Reagent (Thermo Fisher) according to the manufacturer's instructions. Cells were pooled from DF or UF regions from 6 wells to obtain enough material. Lysates were analysed by SDS-PAGE and immunoblotting. Membranes were incubated with primary antibodies (see Table S1)

overnight at 4°C and visualised with HRP-conjugated anti-IgG secondary antibodies and enhanced chemiluminescence substrates (Bio-Rad). The expression of PDHX or calnexin was used as a loading control. For transparency, representative blots are included in Supplementary Fig. 9.

Immunofluorescent staining

EC were fixed in paraformaldehyde (4%) for 20 min, permeabilised with Triton X-100 (0.1%) for 3 min and blocked with BSA (5%) for 1h before incubating with primary antibodies overnight at 4°C (see Table S1). Immunostaining was visualised using relevant Alexa Fluor 488- or 568-conjugated secondary antibodies. In a subset of experiments, EC were incubated with Alexa Fluor-488 Phalloidin (Thermo Fisher) for 20 min at room temperature to visualise the actin cytoskeleton. Nuclei were stained by incubation with DRAQ5 (5 µM). EC were imaged directly in the well using a Leica SP5 or SP8 Laser Scanning Confocal Microscope with excitation at 488, 565 and 633 nm respectively. A minimum of 4 fields of view were studied for each flow condition in each well using identical laser power and detector gain settings. Cell elongation was quantified by calculating the length-to-width ratio. ZO-1 expression within cell junctions was quantified by measuring mean fluorescence intensity within standardised regions of interest spanning cell junctions.

Quantification of EC permeability

EC were seeded in 6-well plates coated with biotinylated gelatin (Dubrovskiy, 2013) and cultured for 72h under static conditions followed by exposure to flow for 72h using the orbital shaker. Medium was replaced with reduced serum (2.5% FBS) EC growth medium (Promocell) for the final 24h of flow exposure. FITC-avidin diluted in reduced serum medium (0.38 µM) was added to wells which were incubated at 37°C for 3 minutes. Binding of fluorescently-labelled avidin to biotin occurs underneath, in particular the intercellular junctions (Ghim, 2017), and can be imaged. Monolayers were washed with PBS to remove unbound tracer before fixing with 4% paraformaldehyde for 10 min. Fixed monolayers were then incubated with an anti-VE-cadherin antibody to delineate cell junctions. Wells were imaged with a Leica SP5 inverted confocal microscope using a x10, 0.40 NA objective. 9 z-stack images were taken from the DF region in the centre of the well (3x3 tile scan) and 12 images from the UF regions at the edge of the well. For quantification of FITC-avidin

accumulation, a max projection image was computed for each stack of images and the tracer fluorescence was distinguished from background noise by intensity and area thresholding. The resulting binarised image was overlaid on the original image and used as a mask to quantify the FITC-avidin accumulation.

Immunostaining and imaging of porcine aortas

Aortic arches were obtained from juvenile pigs (<16 weeks of age) culled at Newman's abattoir (Farnborough, Surrey) or from The Pirbright Institute (Pirbright, UK). Tissue obtained from The Pirbright Institute was collected in accordance with Directive 2010/63/EU of the European Parliament on the protection of animals used for scientific purposes, under authorisation of the UK Home Office (Project License No. 70/8852) and the Animal Welfare and Ethical Review Board (AWERB) of The Pirbright Institute (Matos, 2022). Pigs were euthanized by overdose of 10ml pentobarbital (Dolethal 200mg/ml solution for injection, Vetoquinol UK Ltd)(Matos, 2022). The aortic arch was excised and fixed immediately in 4% paraformaldehyde for up to 7 days. Aortas were dissected into 1cm² sections from either the inner or outer curvature, exposed to disturbed or undisturbed flow according to previous computational fluid dynamic analysis (Serbanovic-Canic, 2017) and the sections were placed into a glass-bottomed 24-well plate. Tissue was permeabilised with Triton X-100 (0.1% v/v) for 5 min before blocking with normal goat serum (10% v/v) for 1 h. It was then stained with β -catenin and FZD4 antibodies (see Table S1) overnight at 4°C for 24 h and 48 h, respectively. Immunostaining was visualised using relevant Alexa Fluor 488- or 568-conjugated secondary antibodies. Nuclei were stained using DAPI (1 $\mu\text{g}\cdot\text{ml}^{-1}$) and tissue was imaged *en face* using a Lecia SP8 confocal microscope with excitation at 405, 488 and 561 nm. A minimum of 4 fields of view were studied for each flow condition using identical laser power and detector gain settings.

Statistical Analysis

All data are presented as mean \pm standard error of the mean (SEM). A minimum of three independent experiments was carried out for each investigation. Cells from at least three independent donors were used for each experiment. Power calculations were carried out

using GraphPad StatMate to ensure 80% power. Data were analysed using GraphPad Prism v9.00. A Shapiro Wilk normality test was used to determine whether data were normally distributed. For normally distributed data, statistical significance was determined using a Student's two-tailed t-test when comparing two conditions or by one- or two-way analysis of variance (ANOVA) with Tukey's multiple comparison test when comparing multiple conditions. Where normalised data are presented, statistical analysis was carried out using a Mann-Whitney test to compare two conditions or Kruskal-Wallis analysis with Dunn's multiple comparison test to compare multiple conditions. For all data * $P < 0.05$, ** $P < 0.01$, *** $P < 0.001$.

Acknowledgments

We are grateful to Dr Paola Campagnolo and Glenda Oliveira from the University of Surrey for collection of pig tissue for FZD4 staining.

Competing interests

No competing interests declared.

Funding

This work was supported by funding from The British Heart Foundation [FS/16/2/31739] to CW and [PG/15/102/31890] to PDW.

References

- Alfaidi, M., Bhattarai, U. and Orr, A.W. (2020) 'Nck1, But Not Nck2, Mediates Disturbed Flow-Induced p21-Activated Kinase Activation and Endothelial Permeability', *Journal of the American Heart Association: Cardiovascular and Cerebrovascular Disease*, **9**(11), 16099.
- Arshad, M., Ghim, M., Mohamied, Y., Sherwin, S.J. and Weinberg, P.D. (2021) 'Endothelial cells do not align with the mean wall shear stress vector', *Journal of the Royal Society, Interface*, **18**(174), 20200772.
- Bian, W.J., Miao, W.Y., He, S.J., Wan, Z.F., Luo, Z.G. and Yu, X. (2015) 'A novel Wnt5a-Frizzled4 signaling pathway mediates activity-independent dendrite morphogenesis via the distal PDZ motif of Frizzled 4', *Developmental Neurobiology*, **75**(8), 805–822.
- Birukov, K.G., Birukova, A.A., Dudek, S.M., Verin, A.D., Crow, M.T., Zhan, X., DePaola, N. and Garcia, J.G.N. (2002) 'Shear stress-mediated cytoskeletal remodeling and cortactin translocation in pulmonary endothelial cells', *American Journal of Respiratory Cell and Molecular Biology*, **26**(4), 453–464.
- Biswas, P., Canosa, S., Schoenfeld, D., Schoenfeld, J., Li, P., Cheas, L.C., Zhang, J., Cordova, A., Sumpio, B. and Madri, J.A. (2006) 'PECAM-1 Affects GSK-3 β -Mediated β -Catenin Phosphorylation and Degradation', *The American Journal of Pathology*, **169**(1), 314–324.
- Bondareva, O., Tsaryk, R., Bojovic, V., Odenthal-Schnittler, M., Siekmann, A.F. and Schnittler, H.-J. (2019) 'Identification of atheroprone shear stress responsive regulatory elements in endothelial cells', *Cardiovascular Research*, **115**(10), 1487–1499.
- Bretón-Romero, R., Feng, B., Holbrook, M., Farb, M.G., Fetterman, J.L., Linder, E.A., Berk, B.D., Masaki, N., Weisbrod, R.M., Inagaki, E., Gokce, N., Fuster, J.J., Walsh, K. and Hamburg, N.M. (2016) 'Endothelial Dysfunction in Human Diabetes Is Mediated by Wnt5a–JNK Signaling', *Arteriosclerosis, Thrombosis, and Vascular Biology*, **36**(3), 561–569.
- Carvalho, J.R., Fortunato, I.C., Fonseca, C.G., Pezzarossa, A., Barbacena, P., Dominguez-Cejudo, M.A., Vasconcelos, F.F., Santos, N.C., Carvalho, F.A. and Franco, C.A. (2019) 'Non-canonical Wnt signaling regulates junctional mechanocoupling during angiogenic collective cell migration', *eLife*, **8**.

Cattelino, A., Liebner, S., Gallini, R., Zanetti, A., Balconi, G., Corsi, A., Bianco, P., Wolburg, H., Moore, R., Oreda, B., Kemler, R. and Dejana, E. (2003) 'The conditional inactivation of the β -catenin gene in endothelial cells causes a defective vascular pattern and increased vascular fragility', *The Journal of Cell Biology*, **162**(6), 1111–1122.

Cho, Y.K., Kang, Y.M., Lee, S.E., Lee, Y. La, Seol, S.M., Lee, W.J., Park, J.Y. and Jung, C.H. (2018) 'Effect of SFRP5 (Secreted Frizzled-Related Protein 5) on the WNT5A (Wingless-Type Family Member 5A)-Induced endothelial dysfunction and its relevance with arterial stiffness in human subjects', *Arteriosclerosis, Thrombosis, and Vascular Biology*, **38**(6), 1358–1367.

Daneman, R., Agalliu, D., Zhou, L., Kuhnert, F., Kuo, C.J. and Barres, B.A. (2009) 'Wnt/ β -catenin signaling is required for CNS, but not non-CNS, angiogenesis', *Proceedings of the National Academy of Sciences*, **106**(2), 641–646.

Davies, P.F., Civelek, M., Fang, Y. and Fleming, I. (2013) 'The atherosusceptible endothelium: endothelial phenotypes in complex haemodynamic shear stress regions in vivo', *Cardiovascular Research*, **99**(2), 315–327.

Descamps, B., Sewduth, R., Ferreira Tojais, N., Jaspard, B., Reynaud, A., Sohet, F., Lacolley, P., Allières, C., Lamazière, J.M.D., Moreau, C., Dufourcq, P., Couffinhal, T. and Dupl a, C. (2012) 'Frizzled 4 regulates arterial network organization through noncanonical Wnt/planar cell polarity signaling', *Circulation Research*, **110**(1), 47–58.

Dijksterhuis, J.P., Petersen, J. and Schulte, G. (2014) 'WNT/Frizzled signalling: receptor-ligand selectivity with focus on FZD-G protein signalling and its physiological relevance: IUPHAR Review 3', *British Journal of Pharmacology*, **171**(5), 1195–1209.

Dubrovskiy, O., Birukova, A.A. and Birukov, K.G. (2013) 'Measurement of local permeability at subcellular level in cell models of agonist- and ventilator-induced lung injury', *Lab Invest*, **93**(2), 254–263.

Dufourcq, P., Leroux, L., Ezan, J., Descamps, B., Lamazière, J.-M.D., Costet, P., Basoni, C., Moreau, C., Deutsch, U., Couffinhal, T. and Dupl a, C. (2008) 'Regulation of Endothelial Cell Cytoskeletal Reorganization by a Secreted Frizzled-Related Protein-1 and Frizzled 4- and Frizzled 7-Dependent Pathway : Role in Neovessel Formation', *The American Journal of Pathology*, **172**(1), 37.

Franco, C.A., Jones, M.L., Bernabeu, M.O., Vion, A.-C., Barbacena, P., Fan, J., Mathivet, T., Fonseca, C.G., Ragab, A., Yamaguchi, T.P., Coveney, P. V, Lang, R.A. and Gerhardt, H. (2016) 'Non-canonical Wnt signalling modulates the endothelial shear stress flow sensor in vascular remodelling', *eLife*, **5**.

Gammons, M. and Bienz, M. (2018) 'Multiprotein complexes governing Wnt signal transduction', *Current Opinion in Cell Biology*, **51**, 42–49.

Gammons, M.V., Renko, M., Johnson, C.M., Rutherford, T.J. and Bienz, M. (2016) 'Wnt Signalosome Assembly by DEP Domain Swapping of Dishevelled', *Molecular Cell*, **64**(1), 92.

Garcia, J.G.N., Liu, F., Verin, A.D., Birukova, A., Dechert, M.A., Gerthoffer, W.T., Bamburg, J.R. and English, D. (2001) 'Sphingosine 1-phosphate promotes endothelial cell barrier integrity by Edg-dependent cytoskeletal rearrangement', *Journal of Clinical Investigation*, **108**(5), 689–701.

Gelfand, B.D., Meller, J., Pryor, A.W., Kahn, M., Bortz, P.D.S., Wamhoff, B.R. and Blackman, B.R. (2011) 'Hemodynamic Activation of β -Catenin and T-Cell-Specific Transcription Factor Signaling in Vascular Endothelium Regulates Fibronectin Expression', *Arteriosclerosis, Thrombosis, and Vascular Biology*, **31**(7), 1625–1633.

Ghim, M., Alpresa, P., Yang, S.W., Braakman, S.T., Gray, S.G., Sherwin, S.J., Van Reeuwijk, M. and Weinberg, P.D. (2017) 'Visualization of three pathways for macromolecule transport across cultured endothelium and their modification by flow', *American Journal of Physiology - Heart and Circulatory Physiology*, **313**(5), H959–H973.

Ghim, M., Pang, K.T., Arshad, M., Wang, X. and Weinberg, P.D. (2018) 'A novel method for segmenting growth of cells in sheared endothelial culture reveals the secretion of an anti-inflammatory mediator', *Journal of Biological Engineering*, **12**(1).

Ghim, M., Yang, S.W., David, K.R.Z., Eustaquio, J., Warboys, C.M. and Weinberg, P.D. (2022) 'NO Synthesis but Not Apoptosis, Mitosis or Inflammation Can Explain Correlations between Flow Directionality and Paracellular Permeability of Cultured Endothelium', *International journal of molecular sciences*, **23**(15).

Givens, C. and Tzima, E. (2016) 'Endothelial Mechanosignaling: Does One Sensor Fit All?', *Antioxidants & redox signaling*, **25**(7), 373–88.

Gonsalves, F.C., Klein, K., Carson, B.B., Katz, S., Ekas, L.A., Evans, S., Nagourney, R., Cardozo, T., Brown, A.M.C. and DasGupta, R. (2011) 'An RNAi-based chemical genetic screen identifies three small-molecule inhibitors of the Wnt/wingless signaling pathway', *Proceedings of the National Academy of Sciences*, **108**(15), 5954–5963.

Gu, Q., Tian, H., Zhang, K., Chen, Deyu, Chen, Dechun, Wang, X. and Zhao, J. (2018) 'Wnt5a/FZD4 Mediates the Mechanical Stretch-Induced Osteogenic Differentiation of Bone Mesenchymal Stem Cells', *Cellular Physiology and Biochemistry*, **48**(1), 215–226.

Hao, H.-X., Xie, Y., Zhang, Y., Charlat, O., Oster, E., Avello, M., Lei, H., Mickanin, C., Liu, D., Ruffner, H., Mao, X., Ma, Q., Zamponi, R., Bouwmeester, T., Finan, P.M., Kirschner, M.W., Porter, J.A., Serluca, F.C. and Cong, F. (2012) 'ZNR3 promotes Wnt receptor turnover in an R-spondin-sensitive manner', *Nature*, **485**(7397), 195–200.

Hao, H.X., Jiang, X. and Cong, F. (2016) 'Control of Wnt Receptor Turnover by R-spondin-ZNR3/RNF43 Signaling Module and Its Dysregulation in Cancer', *Cancers*, **8**(6).

Hu, Y., Chen, M., Wang, M. and Li, X. (2021) 'Flow-mediated vasodilation through mechanosensitive G protein-coupled receptors in endothelial cells', *Trends in Cardiovascular Medicine* [Preprint]. Elsevier Inc.

Huveneers, S., Oldenburg, J., Spanjaard, E., van der Krogt, G., Grigoriev, I., Akhmanova, A., Rehmann, H. and de Rooij, J. (2012) 'Vinculin associates with endothelial VE-cadherin junctions to control force-dependent remodeling', *Journal of Cell Biology*, **196**(5), 641–652.

Koo, B.-K., Spit, M., Jordens, I., Low, T.Y., Stange, D.E., van de Wetering, M., van Es, J.H., Mohammed, S., Heck, A.J.R., Maurice, M.M. and Clevers, H. (2012) 'Tumour suppressor RNF43 is a stem-cell E3 ligase that induces endocytosis of Wnt receptors', *Nature*, **488**(7413), 665–669.

Lai, S.-L., Chien, A.J. and Moon, R.T. (2009) 'Wnt/Fz signaling and the cytoskeleton: potential roles in tumorigenesis', *Cell Research 2009 19:5*, **19**(5), 532–545.

Li, R., Beebe, T., Jen, N., Yu, F., Takabe, W., Harrison, M., Cao, H., Lee, J., Yang, H., Han, P., Wang, K., Shimizu, H., Chen, J., Lien, C.-L., Chi, N.C. and Hsiai, T.K. (2014) 'Results OSS Activated Ang-2 Expression via Wnt Signaling', *Arteriosclerosis, Thrombosis, and Vascular Biology*, **34**(10), 2268.

Liebner, S., Cattelino, A., Gallini, R., Rudini, N., Iurlaro, M., Piccolo, S. and Dejana, E. (2004) 'β-Catenin is required for endothelial-mesenchymal transformation during heart cushion development in the mouse', *Journal of Cell Biology*, **166**(3), 359–367.

Lu, W., Yamamoto, V., Ortega, B. and Baltimore, D. (2004) 'Mammalian Ryk Is a Wnt Coreceptor Required for Stimulation of Neurite Outgrowth', *Cell*, **119**(1), 97–108.

Lyu, Q., Xu, S., Lyu, Y., Choi, M., Christie, C.K., Slivano, O.J., Rahman, A., Jin, Z.G., Long, X., Xu, Y. and Miano, J.M. (2019) 'SENCr stabilizes vascular endothelial cell adherens junctions through interaction with CKAP4', *Proceedings of the National Academy of Sciences of the United States of America*, **116**(2), 546–555.

MacDonald, B.T., Tamai, K. and He, X. (2009) 'Wnt/β-catenin signaling: components, mechanisms, and diseases.', *Developmental cell*, **17**(1), 9–26.

Mahmoud, M.M., Kim, H.R., Xing, R., Hsiao, S., Mammoto, A., Chen, J., Serbanovic-Canic, J., Feng, S., Bowden, N.P., Maguire, R., Ariaans, M., Francis, S.E., Weinberg, P.D., Van Der Heiden, K., Jones, E.A., Chico, T.J.A., Ridger, V. and Evans, P.C. (2016) 'TWIST1 integrates endothelial responses to flow in vascular dysfunction and atherosclerosis', *Circulation Research*, **119**(3), 450–462.

Mahmoud, M.M., Serbanovic-Canic, J., Feng, S., Souilhol, C., Xing, R., Hsiao, S., Mammoto, A., Chen, J., Ariaans, M., Francis, S.E., Van Der Heiden, K., Ridger, V. and Evans, P.C. (2017) 'Shear stress induces endothelial- to-mesenchymal transition via the transcription factor Snail', *Scientific Reports*, **7**, 3375.

Maimari, N., Pedrigi, R.M., Russo, A., Broda, K. and Krams, R. (2016) 'Integration of flow studies for robust selection of mechanoresponsive genes', *Thromb Haemost*, **115**(3), 474–483.

Matos, R.S., Maselli, D., McVey, J.H., Heiss, C. and Campagnolo, P. (2022) '3D Printed Bioreactor Enabling the Pulsatile Culture of Native and Angioplastied Large Arteries', *Frontiers in Cardiovascular Medicine*, **9**, 864580.

McCue, S., Noria, S. and Langille, B.L. (2004) 'Shear-induced reorganization of endothelial cell cytoskeleton and adhesion complexes', *Trends in Cardiovascular Medicine*. Elsevier Inc., 143–151.

Mikels, A.J. and Nusse, R. (2006) 'Purified Wnt5a protein activates or inhibits β -catenin-TCF signaling depending on receptor context', *PLoS Biology*, **4**(4), 570–582.

Mohamied, Y., Rowland, E.M., Bailey, E.L., Sherwin, S.J., Schwartz, M.A. and Weinberg, P.D. (2015) 'Change of Direction in the Biomechanics of Atherosclerosis', *Annals of Biomedical Engineering*, **43**(1), 16–25.

Ni, C.-W., Qiu, H., Rezvan, A., Kwon, K., Nam, D., Son, D.J., Visvader, J.E. and Jo, H. (2010) 'Discovery of novel mechanosensitive genes in vivo using mouse carotid artery endothelium exposed to disturbed flow', *Blood*, **116**(15), e66–e73.

Pang, K.T., Ghim, M., Liu, C., Tay, H.M., Fhu, C.W., Chia, R.N., Qiu, B., Sarathchandra, P., Chester, A.H., Yacoub, M.H., Wilkinson, F.L., Weston, R., Warboys, C.M., Hou, H.W., Weinberg, P.D. and Wang, X. (2021) 'Leucine-Rich α -2-Glycoprotein 1 Suppresses Endothelial Cell Activation Through ADAM10-Mediated Shedding of TNF- α Receptor', *Frontiers in Cell and Developmental Biology*, **0**, 1743.

Peiffer, V., Sherwin, S.J. and Weinberg, P.D. (2013) 'Does low and oscillatory wall shear stress correlate spatially with early atherosclerosis? A systematic review', *Cardiovascular Research*, **99**(2), 242–250.

Pereira, C., Schaer, D.J., Bachli, E.B., Kurrer, M.O. and Schoedon, G. (2008) 'Wnt5A/CaMKII signaling contributes to the inflammatory response of macrophages and is a target for the antiinflammatory action of activated protein C and interleukin-10.', *Arteriosclerosis, thrombosis, and vascular biology*, **28**(3), 504–10.

Scholz, B., Korn, C., Wojtarowicz, J., Mogler, C., Augustin, I., Boutros, M., Niehrs, C. and Augustin, H.G. (2016) 'Endothelial RSPO3 Controls Vascular Stability and Pruning through Non-canonical WNT/Ca²⁺/NFAT Signaling', *Developmental Cell*, **36**(1), 79–93.

Serbanovic-Canic, J., De Luca, A., Warboys, C., Ferreira, P.F., Luong, L.A., Hsiao, S., Gauci, I., Mahmoud, M., Feng, S., Souilhol, C., Bowden, N., Ashton, J.-P., Walczak, H., Firmin, D., Krams, R., Mason, J.C., Haskard, D.O., Sherwin, S., Ridger, V., Chico, T.J.A. and Evans, P.C. (2017) 'Zebrafish model for functional screening of flow-responsive genes', *Arteriosclerosis, Thrombosis, and Vascular Biology*, **37**(1).

- Shikata, Y., Birukov, K.G. and Garcia, J.G.N. (2003) 'S1P induces FA remodeling in human pulmonary endothelial cells: Role of Rac, GIT1, FAK, and paxillin', *Journal of Applied Physiology*, **94**(3), 1193–1203.
- Skaria, T., Bachli, E. and Schoedon, G. (2017) 'Wnt5A/Ryk signaling critically affects barrier function in human vascular endothelial cells', *Cell Adhesion & Migration*, **11**(1), 24–38.
- Skaria, T., Bachli, E. and Schoedon, G. (2018) 'RSPO3 impairs barrier function of human vascular endothelial monolayers and synergizes with pro-inflammatory IL-1', *Molecular Medicine 2018 24:1*, **24**(1), 1–7.
- Suo, J., Ferrara, D.E., Sorescu, D., Guldberg, R.E., Taylor, W.R. and Giddens, D.P. (2007) 'Hemodynamic shear stresses in mouse aortas: Implications for atherogenesis', *Arteriosclerosis, Thrombosis, and Vascular Biology*, **27**(2), 346–351.
- Tajadura, V., Hansen, M.H., Smith, J., Charles, H., Rickman, M., Farrell-Dillon, K., Claro, V., Warboys, C. and Ferro, A. (2020) ' β -catenin promotes endothelial survival by regulating eNOS activity and flow-dependent anti-apoptotic gene expression', *Cell Death & Disease 2020 11:6*, **11**(6), 1–16.
- Tornavaca, O., Chia, M., Dufton, N., Almagro, L.O., Conway, D.E., Randi, A.M., Schwartz, M.A., Matter, K. and Balda, M.S. (2015) 'ZO-1 controls endothelial adherens junctions, cell-cell tension, angiogenesis, and barrier formation', *Journal of Cell Biology*, **208**(6), 821–838.
- Tran, K.A., Zhang, X., Predescu, D., Huang, X., MacHado, R.F., Göthert, J.R., Malik, A.B., Valyi-Nagy, T. and Zhao, Y.Y. (2016) 'Endothelial β -Catenin Signaling Is Required for Maintaining Adult Blood-Brain Barrier Integrity and Central Nervous System Homeostasis', *Circulation*, **133**(2), 177–186.
- Wang, C., Lu, H. and Alexander Schwartz, M. (2012) 'A novel in vitro flow system for changing flow direction on endothelial cells', *Journal of Biomechanics*, **45**(7), 1212–1218.
- Warboys, C., de Luca, A., Amini, N., Luong, L., Duckles, H., Hsiao, S., White, A., Biswas, S., Khamis, R., Chong, C.K., Cheung, W.M., Sherwin, S.J., Bennett, M.R., Gil, J., Mason, J.C., Haskard, D.O. and Evans, P.C. (2014) 'Disturbed flow promotes endothelial senescence via a p53-dependent pathway', *Arteriosclerosis, Thrombosis, and Vascular Biology*, **34**(5), 985–995.

Warboys, C.M. (2018) 'Mechanoactivation of Wnt/ β -catenin pathways in health and disease', *Emerging Topics in Life Sciences*, **2**(5), 701–712.

Warboys, C.M., Chen, N., Zhang, Q., Shaifta, Y., Vanderslott, G., Passacuale, G., Hu, Y., Xu, Q., Ward, J.P.T. and Ferro, A. (2014) 'Bidirectional cross-regulation between the endothelial nitric oxide synthase and β -catenin signalling pathways', *Cardiovascular Research*, **104**(1), 116–126.

Warboys, C.M., Ghim, M. and Weinberg, P.D. (2019) 'Understanding mechanobiology in cultured endothelium: A review of the orbital shaker method', *Atherosclerosis*, **285**, 170–177.

Wu, C., Huang, R.T., Kuo, C.H., Kumar, S., Kim, C.W., Lin, Y.C., Chen, Y.J., Birukova, A., Birukov, K.G., Dulin, N.O., Civelek, M., Lusic, A.J., Loyer, X., Tedgui, A., Dai, G., Jo, H. and Fang, Y. (2015) 'Mechanosensitive PPAP2B regulates endothelial responses to atherorelevant hemodynamic forces', *Circulation Research*, **117**(4), e41–e53.

Yang, F., Zhang, Y., Zhu, J., Wang, J., Jiang, Z., Zhao, C., Yang, Q., Huang, Y., Yao, W., Pang, W., Han, L. and Zhou, J. (2020) 'Laminar Flow Protects Vascular Endothelial Tight Junctions and Barrier Function via Maintaining the Expression of Long Non-coding RNA MALAT1', *Frontiers in bioengineering and biotechnology*, **8**.

Figures

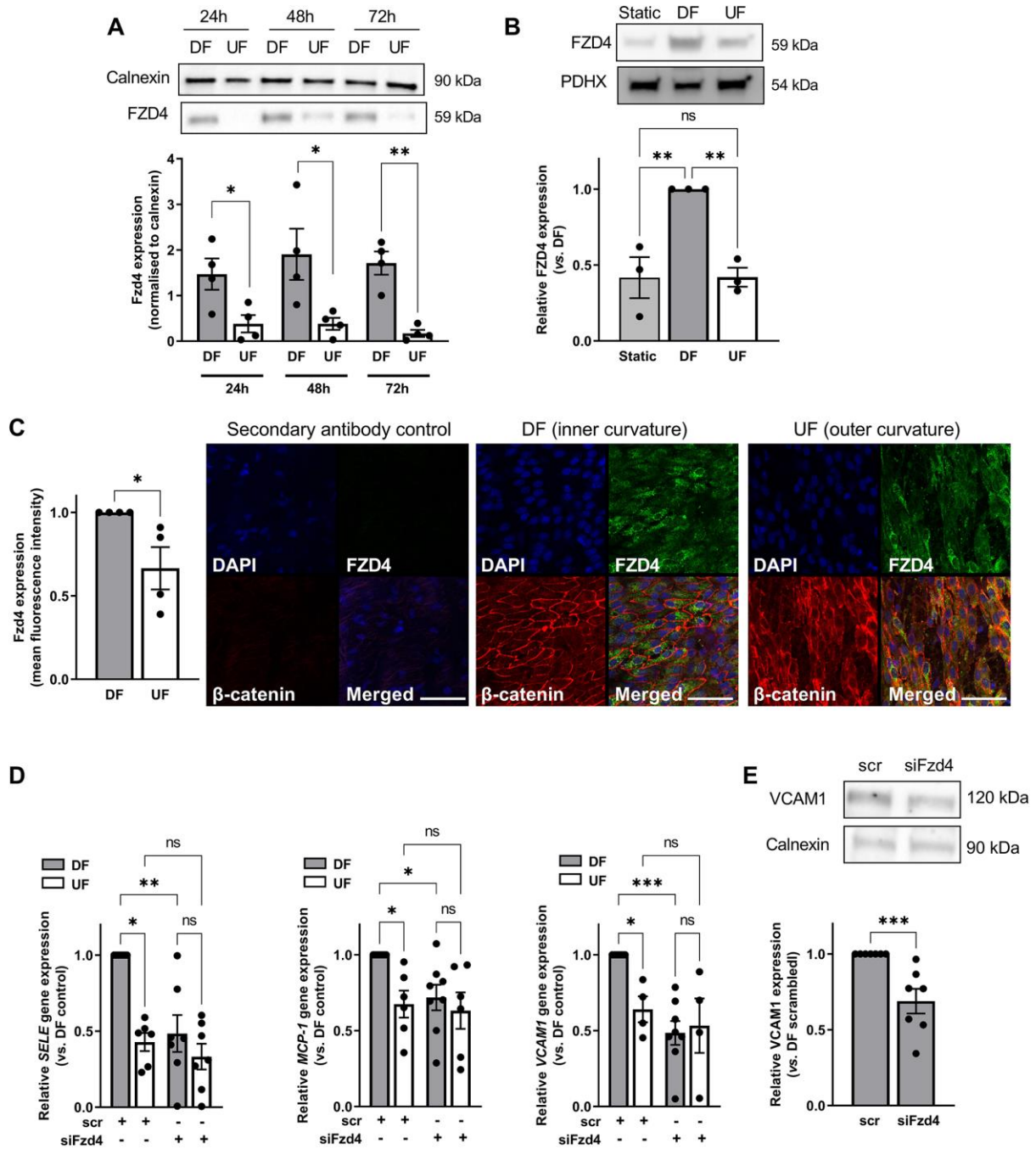


Fig. 1. FZD4 expression is increased in EC exposed to disturbed flow and regulates pro-inflammatory signalling

(A) Protein lysates were obtained from HAEC exposed to DF and UF for 24-72h or **(B)** from HAEC exposed to DF, UF or static conditions for 72h. **(A-B)** FZD4 expression was analysed by western blot using **(A)** calnexin or **(B)** PDHX as a loading control. Data were analysed by **(A)** paired t-test at each time point (n=4) or **(B)** one-way ANOVA (n=3). Representative blots shown in panel above. **(C)** Aortas from juvenile pigs were fixed and sections cut from regions exposed to DF or UF. Sections were stained with anti-FZD4 and anti- β -catenin antibodies. Nuclei were stained with DAPI. Tissue sections were imaged *en face* and mean fluorescence intensity quantified in three fields of view for each flow region (n=4; analysis by Mann-Whitney test; representative images shown; scale = 50 μ m). **(D)** RNA or **(E)** protein lysates were prepared from EC transfected with FZD4 siRNA (siFzd4) or scrambled controls and exposed to DF or UF for 48h. **(D)** Gene expression was determined by qRT-PCR using *GAPDH* as a housekeeping gene (n=6-8; analysis by Kruskal-Wallis test). **(E)** Expression of VCAM1 was assessed by western blot using calnexin as a loading control (n=7; analysis by Mann-Whitney test; representative blots shown in the panel). All data presented as mean \pm s.e.m and all n numbers represent independent biological replicates. All t-tests were two-tailed. *P<0.05, **P<0.01, ***P<0.001.

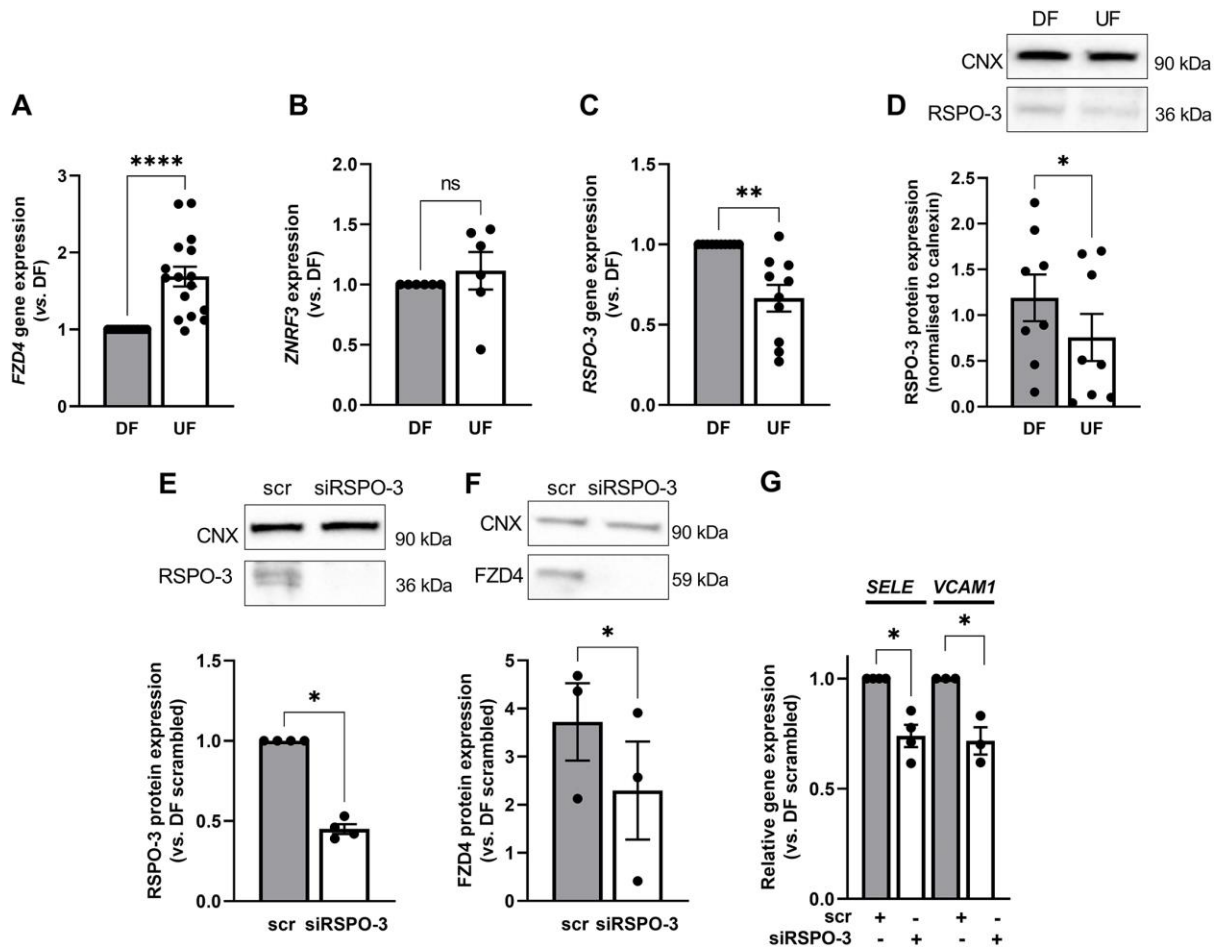


Fig. 2. RSPO-3 expression is increased in EC exposed to disturbed flow and regulates the expression of FZD4.

(A-D) Lysates were obtained from HAEC exposed to DF and UF for 72h. **(A-C)** RNA lysates were prepared and the expression of **(A)** *FZD4* (n=16), **(B)** *ZNRF3* (n=6) and **(C)** *RSPO-3* (n=10) was determined by qRT-PCR using *GAPDH* as a housekeeping gene (analysis by Wilcoxon matched pairs signed rank test). **(D)** Protein lysates were prepared and analysed by western blot using an anti-*RSPO-3* antibody. Calnexin was used as a loading control (n=8; analysis by paired t-test; representative blots shown in the panel above). **(E-G)** HAEC were transfected with *RSPO-3* siRNA (siRSPO-3) or scrambled controls and exposed to flow for 48h. **(E-F)** Protein lysates were prepared from EC exposed to DF and analysed by western blot using **(E)** *RSPO-3* and **(F)** *FZD4* antibodies. Calnexin was used as a loading control (n=3-4; analysis by Mann-Whitney test; representative blots shown in the panels above). **(G)** RNA

was isolated from EC exposed to DF and expression of pro-inflammatory genes determined by qRT-PCR using *GAPDH* as a housekeeping gene (n=3-4; analysis by Mann-Whitney test). All data presented as mean \pm s.e.m and all n numbers represent independent biological replicates. All t-tests were two-tailed. *P<0.05, **P<0.01, ***P<0.001.

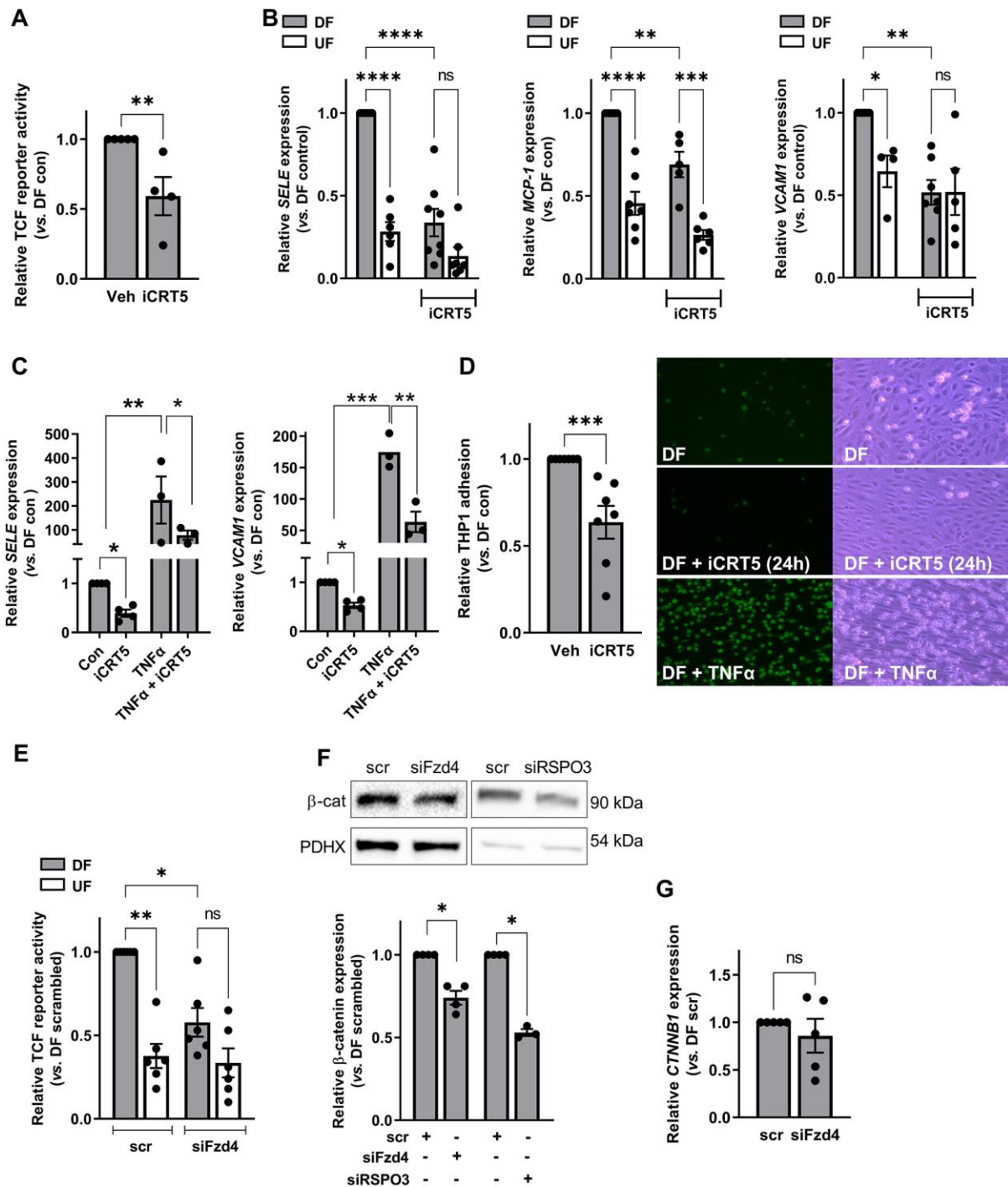


Fig. 3. β -catenin activity is increased in EC exposed to disturbed flow in a FZD4 dependent manner

(A-D) HAEC were exposed to flow for 72h and treated with iCRT5 (50 μ M) for the last 24h of flow exposure. (A) HAEC were transfected with TCF reporter constructs 24h prior to flow exposure. Lysates were prepared from cells exposed to DF and *Firefly* and *Renilla* luciferase

activity recorded. Ratios were corrected for protein content of lysates. Results shown relative to DF control (n=4; analysis by Mann Whitney t-test). **(B-C)** RNA was harvested from EC exposed to DF and UF and gene expression determined by qRT-PCR using *GAPDH* as a housekeeping gene (n=4-8; analysis by two-way ANOVA with Tukey's multiple comparison test). **(C)** HAEC were treated with TNF α for the final 24h of flow exposure. RNA was harvested from EC exposed to DF (n=3-4; analysis by one-way ANOVA) **(D)** The number of adherent calcein-labelled THP-1 monocytes was determined in 4 fields of view following treatment with iCRT5 for the final 24h of flow exposure or for the full duration. Representative fluorescent images for DF control, iCRT5 (24h) and TNF α (positive control) are shown; phase contrast images also included to show presence of intact EC monolayer. Results shown relative to untreated controls (n=7; analysis by Mann-Whitney test). **(E)** HAEC were transfected with FZD4 siRNA (siFzd4) or scrambled control plus TCF reporter constructs and exposed to flow for 48h. Lysates were prepared as for (A). Results shown relative to DF control (n=6; analysis by Kruskal-Wallis test). **(F-G)** HAEC were transfected with FZD4 or RSPO-3 siRNA or scrambled control and exposed to flow for 48h. **(F)** Lysates were prepared from EC exposed to DF and analysed by western blot using an anti- β -catenin antibody. PDHX was used as a loading control (n=3-4; analysis by Mann Whitney test). **(G)** Transcript levels of β -catenin were assessed by qRT-PCR using *GAPDH* as a housekeeping gene (n=5; analysis by Mann Whitney test). All data presented as mean \pm s.e.m and all n numbers represent independent biological replicates. All t-tests were two-tailed. *P<0.05, **P<0.01, ***P<0.001.

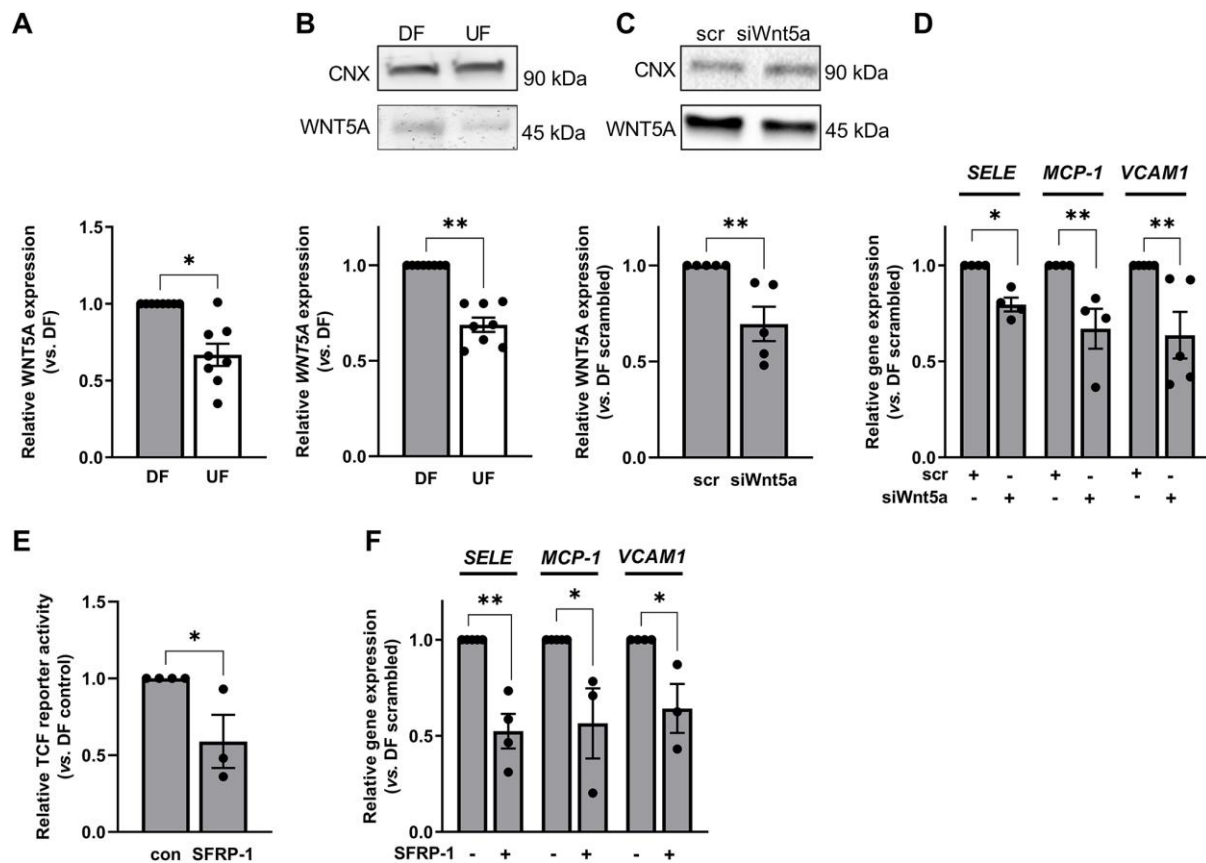


Fig. 4. WNT5A expression is increased in EC exposed to disturbed flow

(A-B) HAEC were exposed to flow for 72h and the expression of WNT5A quantified in cells exposed to DF or UF by **(A)** qRT-PCR using *GAPDH* as a housekeeping gene (n=8; analysis by Wilcoxon signed rank test) or **(B)** western blot using an anti-WNT5A antibody. Calnexin was used as a loading control (n=8; analysis by Wilcoxon signed rank test). **(C-D)** HAEC were transfected with WNT5A siRNA (siWnt5a) or scrambled controls and exposed to flow for 48h. **(C)** WNT5A expression was assessed by western blot using calnexin as a loading control (n=5; analysis by Mann-Whitney test). **(D)** Gene expression was determined by qRT-PCR using *GAPDH* as a housekeeping gene (n=4-5; analysis by Mann-Whitney test). **(E-F)** HAEC were exposed to flow for 72h in the presence of sFRP-1 (200 $\mu\text{g}\cdot\text{ml}^{-1}$) for the duration of flow exposure. **(E)** HAEC were transfected with TCF reporter constructs 24h prior to flow exposure. Lysates were prepared from cells exposed to DF and *Firefly* and *Renilla* luciferase activity recorded. Ratios were corrected for protein content of lysates. Results shown relative to DF control (n=3; analysis by Mann-Whitney test). **(F)** Gene expression was determined by qRT-PCR using *GAPDH* as a housekeeping gene (n=3-4; analysis by Mann-Whitney test). All data presented as mean \pm s.e.m and all n numbers represent independent biological replicates. All t-tests were two-tailed. *P<0.05, **P<0.01, ***P<0.001.

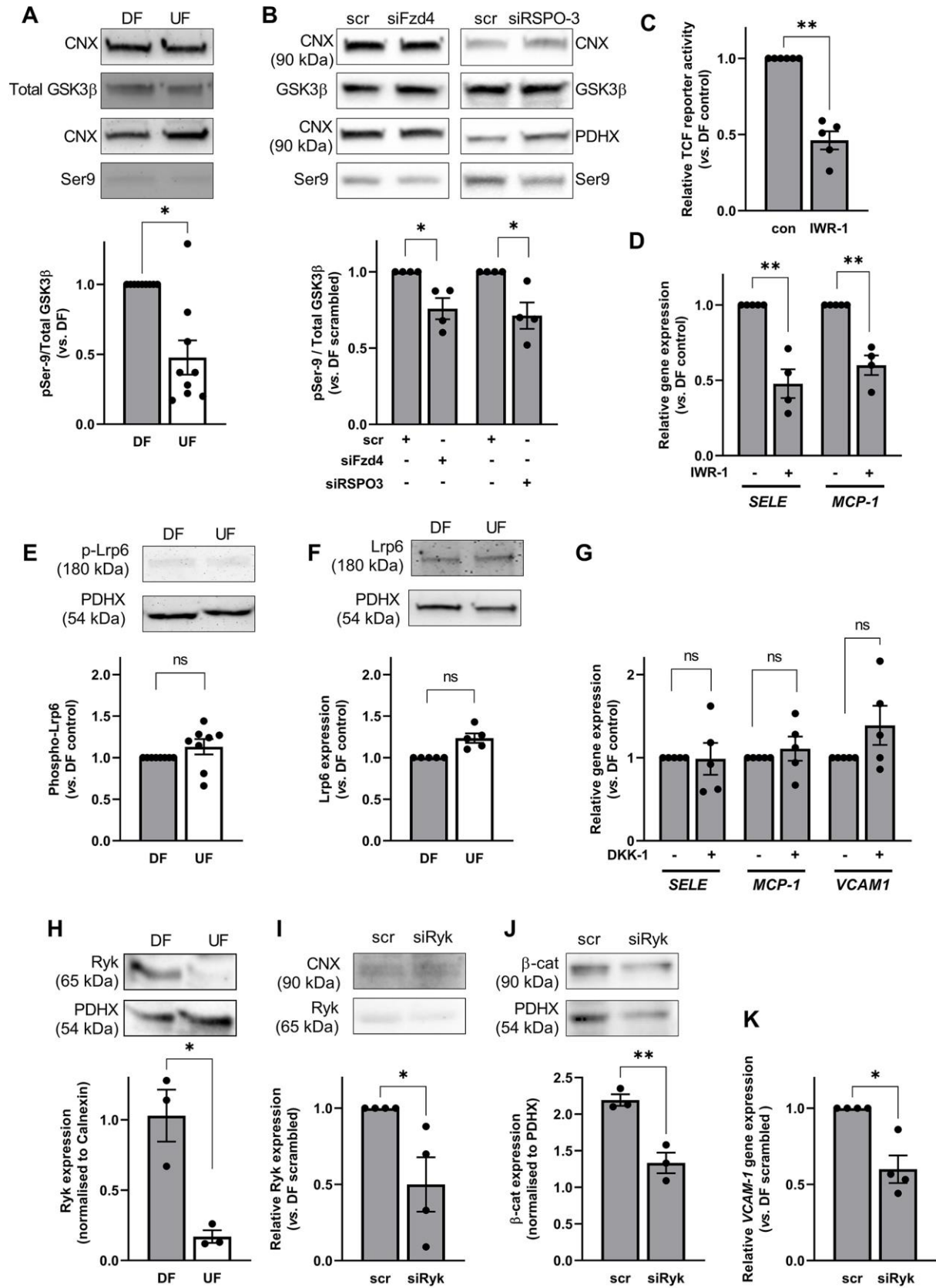


Fig. 5. Disturbed flow inhibits the β -catenin destruction complex in a FZD4 and RSPO-3 and Ryk-dependent manner.

(A-B) GSK3 β phosphorylation was quantified by western blot using anti-phospho Ser9 and anti-GSK3 β (total) antibodies in protein lysates from HAEC exposed to **(A)** DF and UF for 72h or **(B)** DF for 48h following transfection with FZD4 or RSPO-3 siRNA or scrambled controls. Calnexin was used as a loading control. Results shown relative to DF control (**A**; n=9; analysis by Wilcoxon signed rank test and **B**; n=4; analysis by Mann-Whitney test). **(C-D)** HAEC were exposed to flow for 72h and IWR-1 (10 μ M) added for the final 24h of flow exposure. **(C)** HAEC were transfected with TCF reporter constructs 24h prior to flow exposure. Lysates were prepared from cells exposed to DF and *Firefly* and *Renilla* luciferase activity recorded. Ratios were corrected for protein content of lysates. Results shown relative to DF control (n=5; analysis by unpaired t-test). **(D)** Gene expression was determined by qRT-PCR using *GAPDH* as a housekeeping gene (n=4; analysis by unpaired t-test). **(E-F)** Lysates were obtained from EC exposed to DF and UF for 72h and **(E)** phosphorylated (n=8) or **(F)** total LRP6 levels (n=5) assessed by western blot using PDHX as a loading control (analysis by Wilcoxon signed rank test). **(G)** HAEC were exposed to flow for 72h and treated with DKK-1 (250 ng.ml⁻¹) for the last 24h of flow exposure. RNA was harvested from EC exposed to DF and gene expression assessed by qRT-PCR using *GAPDH* as a housekeeping gene (n=4-5; analysis by Mann-Whitney test). **(H)** Lysates were obtained from HAEC exposed to DF and UF for 72h or **(I-K)** from HAEC exposed to DF for 48h following transfection with Ryk siRNA (siRyk) or scrambled controls. **(H-J)** Expression of proteins was determined by western blot using antibodies targeting **(H-I)** Ryk (n=3-4) or **(J)** β -catenin (n=3). PDHX or calnexin was used as a loading control (representative blots shown in the panels above; n=3-4; analysis by Mann-Whitney test). **(K)** *VCAM1* expression was assessed by qRT-PCR using *GAPDH* as a housekeeping gene (n=4; analysis by Mann-Whitney test). All data presented as mean \pm s.e.m and all n numbers represent independent biological replicates. All t-tests were two-tailed. *P<0.05, **P<0.01, ***P<0.001.

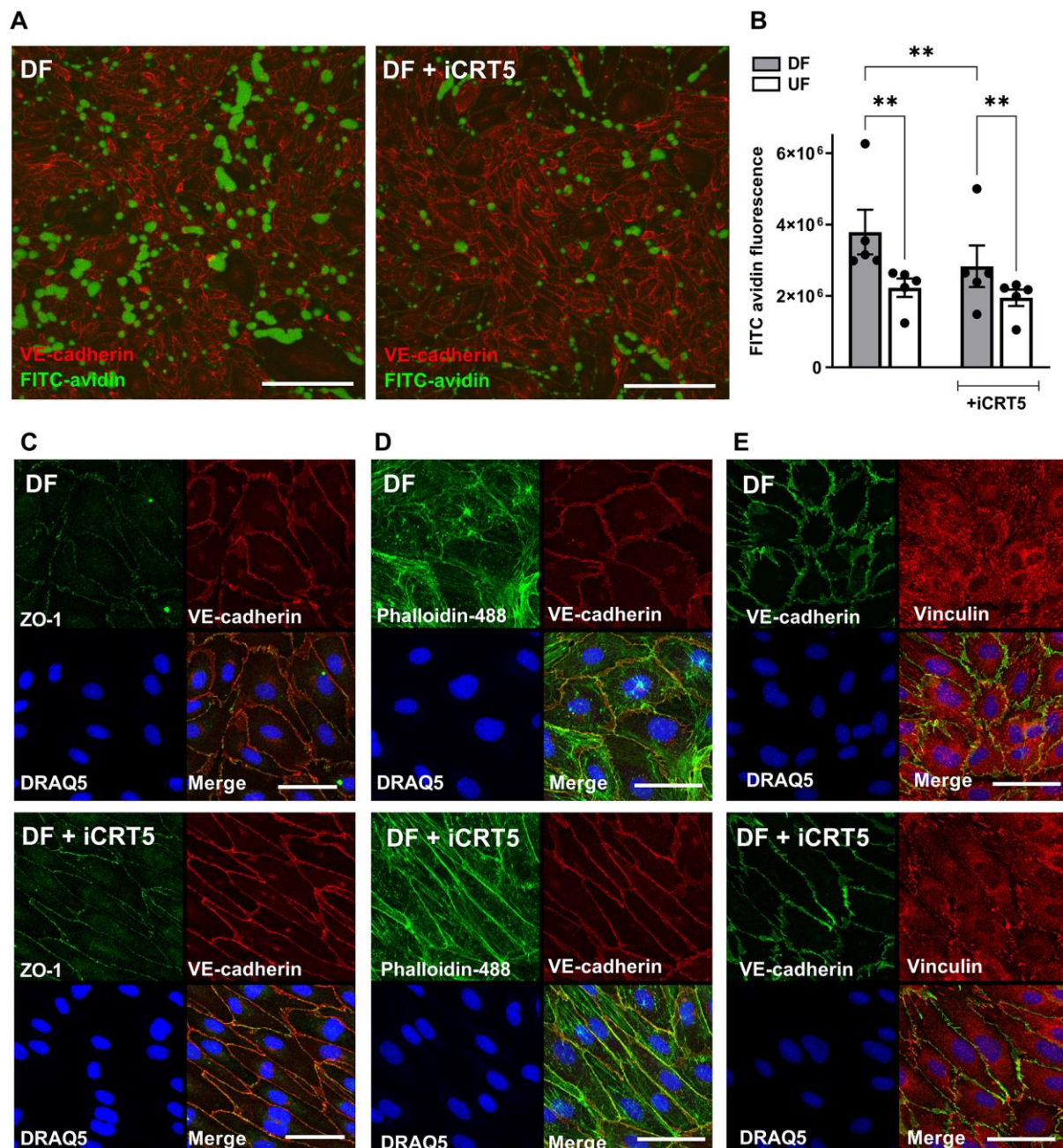


Fig. 6. β -catenin activity increases permeability in EC exposed to disturbed flow and alters cytoskeletal and junctional organisation

(A-E) HAEC were exposed to flow for 72h and treated with iCRT5 (50 μ M) for the last 24h of flow exposure. **(A)** FITC-avidin was added to monolayers immediately after flow cessation. Images show areas where FITC-avidin binds to biotinylated-gelatin underlying EC. Cells were counterstained with an anti-VE-cadherin antibody (images shown are maximum projections of z-stacks; scale = 200 μ m). **(B)** Accumulation of FITC-avidin was quantified by determining

the intensity of FITC-avidin in maximum projections and shown relative to DF vehicle control (n=5; analysis by 2-way ANOVA with Tukey's multiple comparison test). **(C-E)** EC were fixed and stained with an anti-VE-cadherin antibody and DRAQ5 nuclear stain plus **(C)** anti-ZO-1 antibody **(D)** 488-Phalloidin **(E)** anti-vinculin antibody (scale = 50µm; representative images from 4 independent experiments). All data presented as mean ± s.e.m and all n numbers represent independent biological replicates. *P<0.05, **P<0.01, ***P<0.001.

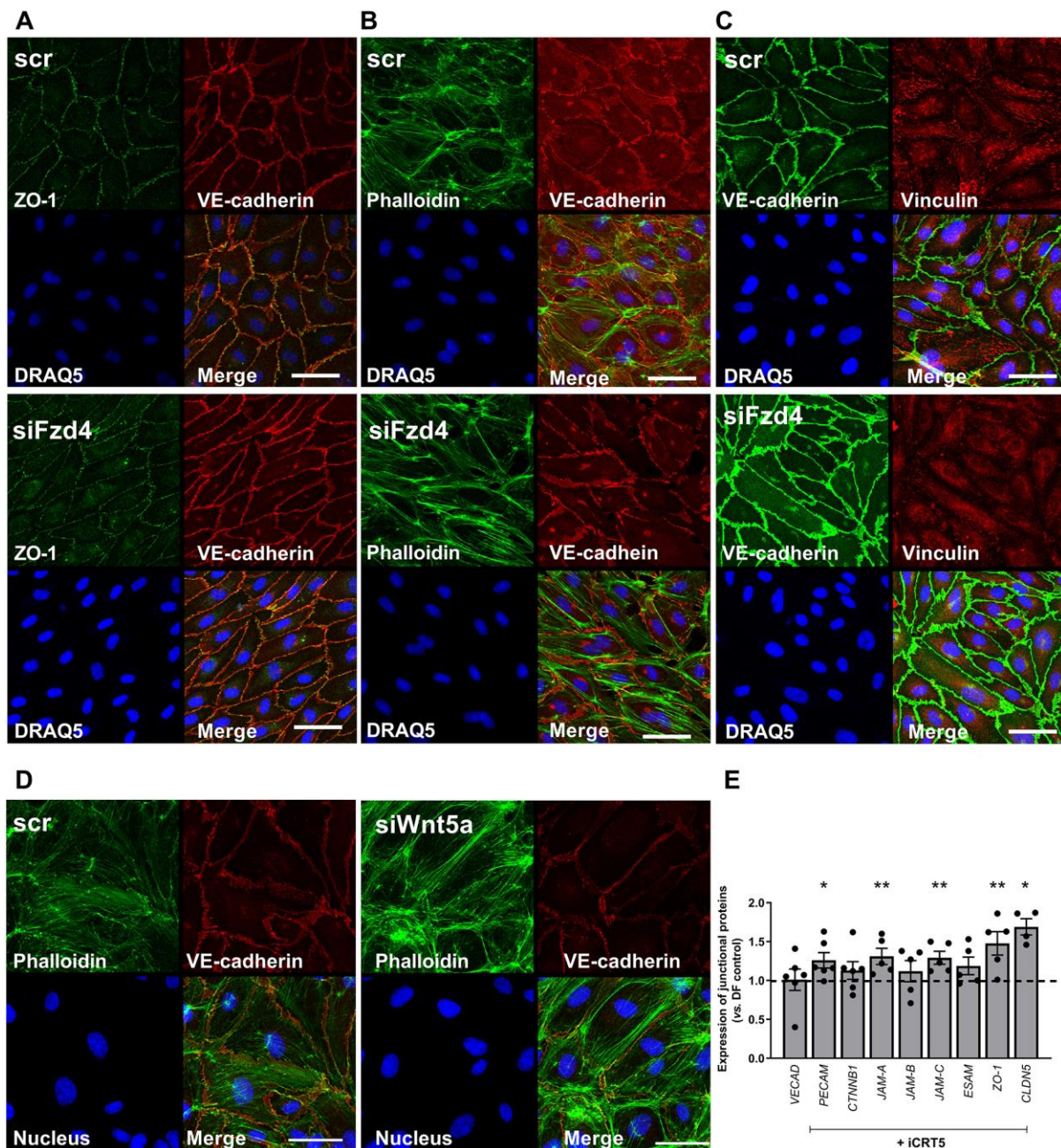


Fig. 7. Knockdown of FZD4 or WNT5A alters organisation of the cytoskeleton and vinculin in EC exposed to disturbed flow

(A-D) HAEC were exposed to disturbed flow for 48h following transfection with siRNA targeting **(A-C)** FZD4 (siFzd4) or **(D)** WNT5A (siWnt5a) and compared to scrambled-transfected control (scr). EC were fixed and stained with an anti-VE-cadherin antibody and DRAQ5 nuclear stain plus **(A)** anti-ZO-1, **(B,D)** 488-Phalloidin or **(C)** anti-vinculin antibody (scale = 50µm; representative images from 4 independent experiments). **(E)** HAEC were

exposed to flow for 72h and treated with iCRT5 (50 μ M) for the last 24h of flow exposure. RNA was harvested from EC exposed to DF and gene expression assessed by qRT-PCR using *GAPDH* as a housekeeping gene (n=4-6; analysis by Mann-Whitney test). All data presented as mean \pm s.e.m and all n numbers represent independent biological replicates. All t-tests were two-tailed. *P<0.05, **P<0.01, ***P<0.001.

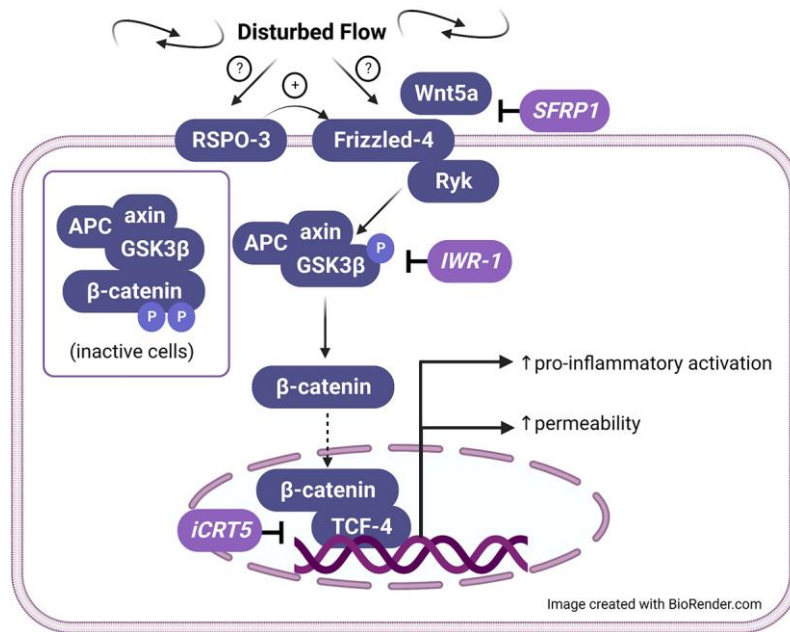


Fig. 8. Proposed pathway of disturbed flow-dependent FZD4-β-catenin signalling

Disturbed flow increases the expression of FZD4 via an RSP0-3 dependent mechanism. Activation of FZD4 by WNT5A inhibits the GSK3β-Axin-APC destruction complex promoting the stabilisation and nuclear translocation of β-catenin. Increased transcriptional activity of β-catenin promotes endothelial dysfunction via increased pro-inflammatory signalling and barrier disruption. The target of inhibitors used in this study is shown at relevant points in the pathway. Image created with BioRender.com.

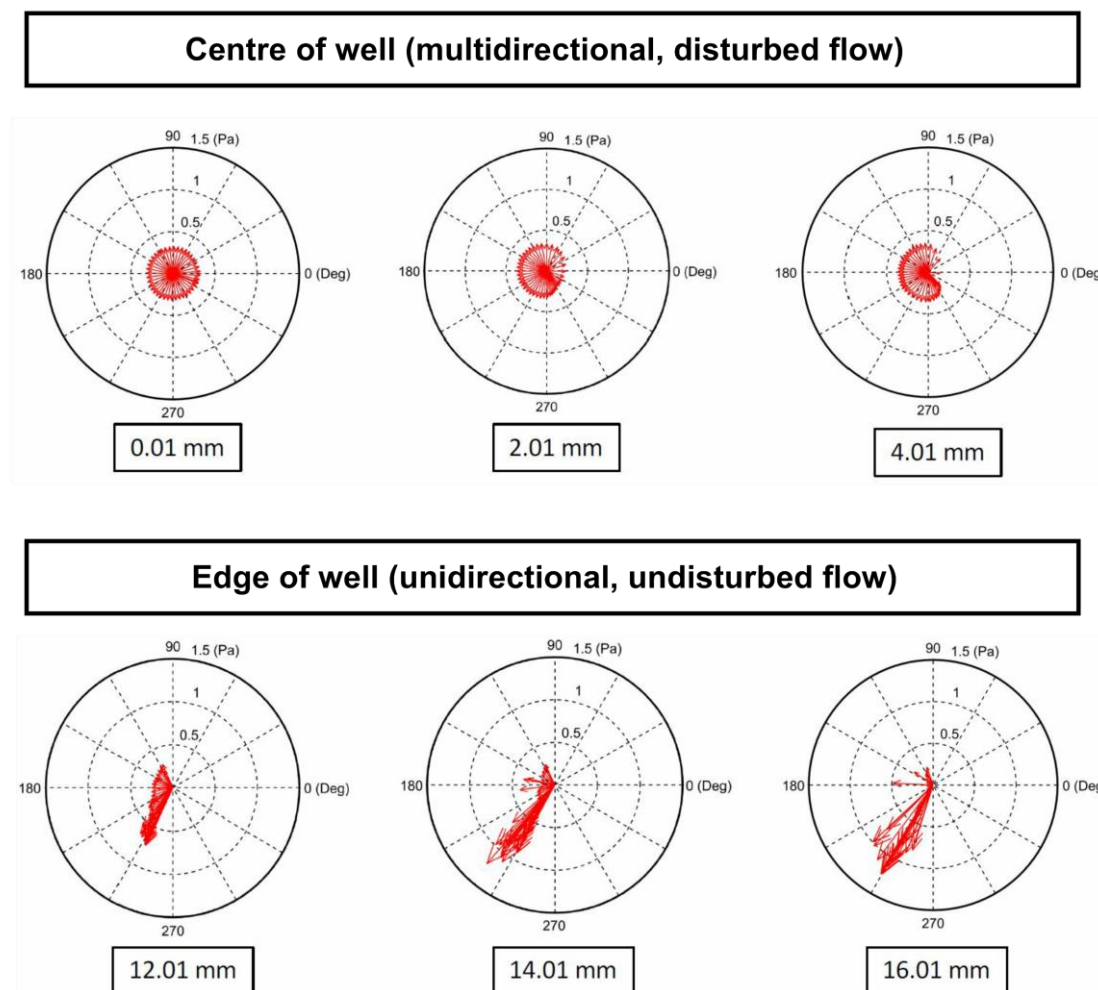


Fig. S1. Polar plots showing direction of WSS vectors in swirling wells

Individual polar plots of the magnitude and direction of instantaneous WSS vectors during one cycle. Each plot applies to one radial distance from the centre of the well. Each arrow represents an instantaneous WSS vector, whose length represents its magnitude, which is plotted at angles corresponding to the shear direction.

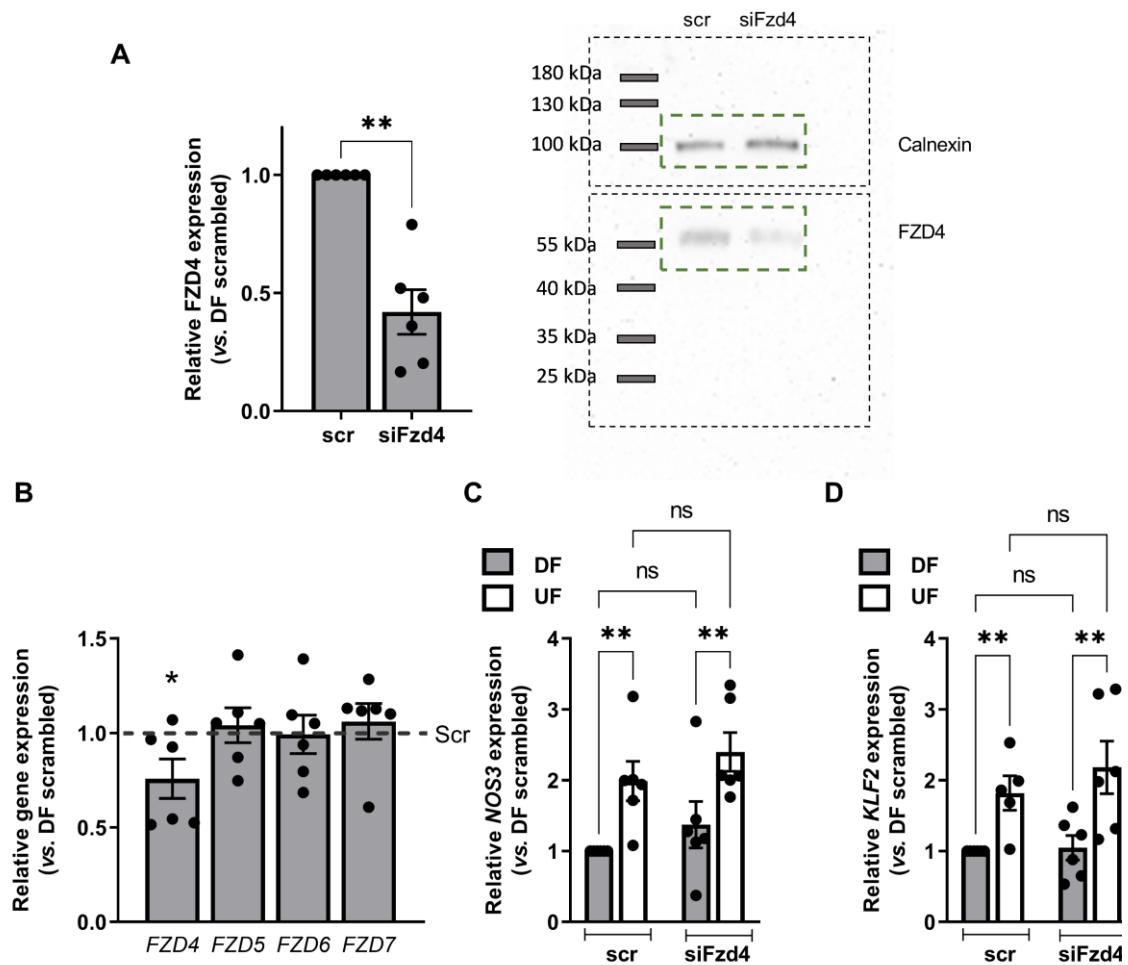


Fig. S2. Efficacy and specificity of Frizzled-4 knockdown using siRNA

(A-D) HAEC were exposed to flow for 48h following transfection with Frizzled-4 siRNA or scrambled controls. (A) Protein lysates were obtained from HAEC exposed to DF and the expression of Frizzled-4 assessed by western blot using calnexin as a loading control (n=6; analysis by Mann-Whitney test). (B) RNA was harvested from EC exposed to DF and the expression of Frizzled-4, Frizzled-5, Frizzled-6 and Frizzled-7 was determined by qRT-PCR using *GAPDH* as a housekeeping gene (n=6; analysis by Mann-Whitney test; results shown relative to DF scrambled control (dashed line)). (C-D) RNA was harvested from EC exposed to DF and UF and the expression of (C) *KLF-2* and (D) *NOS3* was determined by qRT-PCR using *GAPDH* as a housekeeping gene (n=6; analysis by two-way ANOVA with Tukey's multiple comparison test; results shown relative to DF scrambled control).

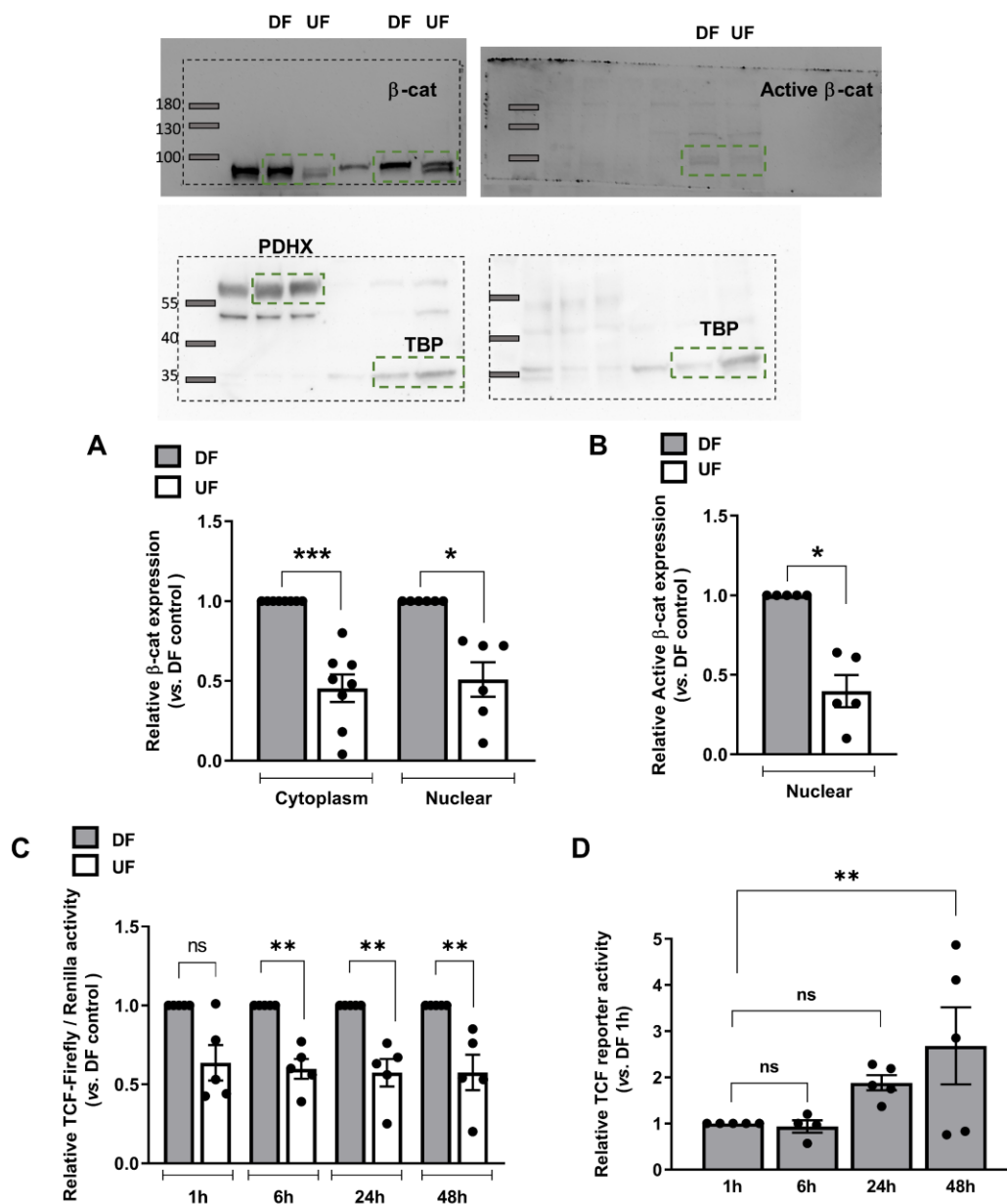


Fig. S3. Disturbed flow increases the expression and activation of β -catenin in human aortic endothelial cells

(A-B) HAEC were exposed to flow for 72h. Lysates were prepared from EC exposed to DF and UF and subject to sub-cellular fractionation. Cytosolic and nuclear fractions were analysed by western blot using **(A)** total β -catenin (n=6-8) and **(B)** active β -catenin antibodies (n=5). PDHX and TBP were used as loading controls for cytosolic and nuclear fractions respectively; analysis by Mann Whitney test; representative blots shown above. **(C)** HAEC were transfected with Cignal TCF/LEF reporter construct prior to flow exposure for 1h – 48h. Lysates were prepared from cells exposed to DF or UF and *Firefly* and *Renilla* luciferase activity was recorded. Ratios were corrected for protein content of lysates. **(C)** Results shown relative to DF control at each time point and analysed by Mann-Whitney test at each time point (n=5). **(D)** Results shown relative to DF 1h and analysed by one-way ANOVA (n=5).

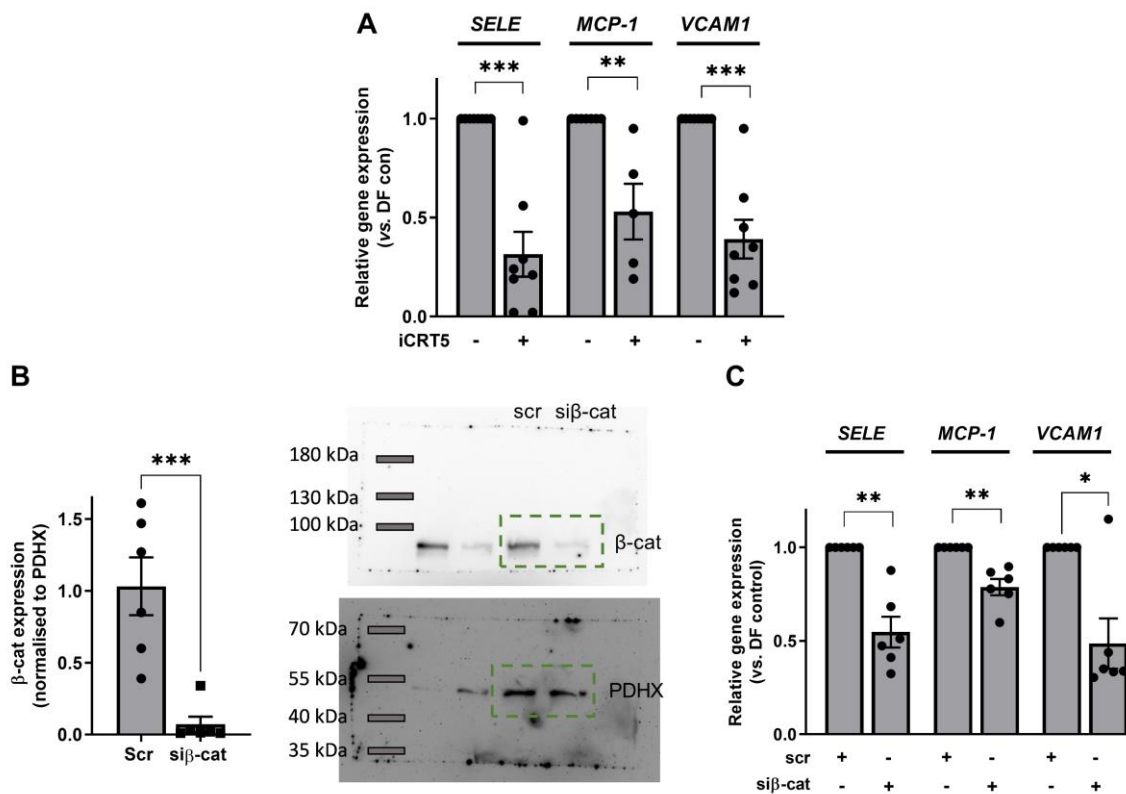


Fig. S4. Expression of pro-inflammatory genes in EC exposed to disturbed flow following inhibition or knockdown of β-catenin

(A) HAEC were exposed to flow for 72h with iCRT5 (50 μM) added for the duration of flow exposure (72h). RNA was harvested from EC exposed to DF and the expression of *E-SEL*, *MCP-1* and *VCAM1* determined by qRT-PCR using *GAPDH* as a housekeeping gene (n=5-8; analysis by Mann-Whitney test). (B-C) HAEC were exposed to flow for 72h following transfection with β-catenin siRNA (siβ-cat). (B) The expression of β-catenin protein was assessed by western blot using PDHX as a loading control (n=6; analysis by analysis by unpaired t-test; representative blot shown next to the graph). (C) RNA was harvested from EC exposed to DF and the expression of pro-inflammatory genes assessed by qRT-PCR using *GAPDH* as a housekeeping gene (n=6; analysis by Mann-Whitney test).

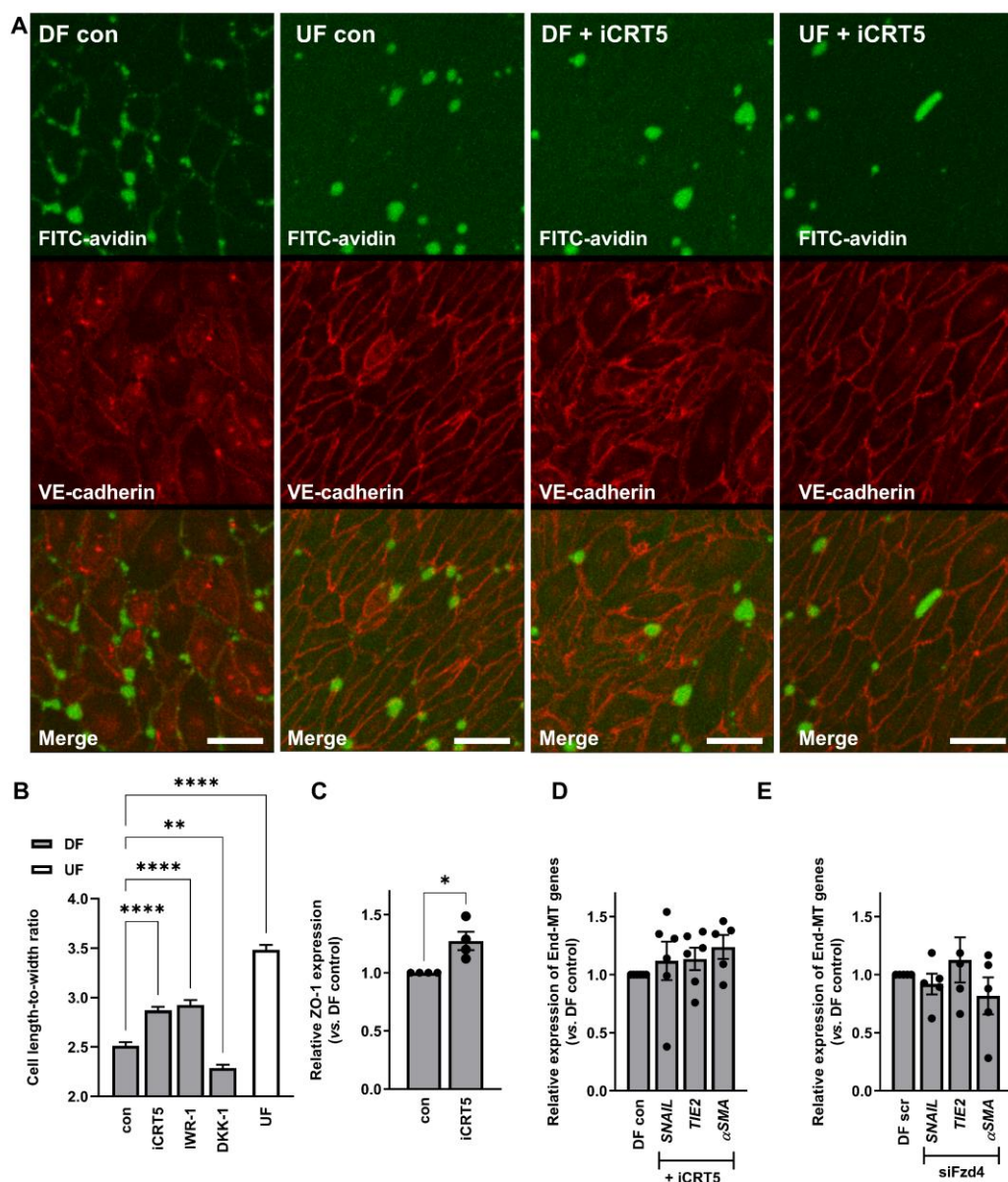


Fig. S5. Permeability and morphology of HAEC

(A) HAEC were cultured on biotinylated-gelatin and exposed to flow for 72h then treated with iCRT5 (50 μ M) for the last 24h of flow exposure. FITC-avidin was added to monolayers immediately after flow cessation. Images show areas where FITC-avidin binds to biotinylated-gelatin underlying EC. Cells were counterstained with an anti-VE-cadherin antibody (images shown are maximum projections of z-stacks; scale = 50 μ m). **(B)** HAEC were fixed and stained with VE-cadherin and DRAQ5 and viewed at x10 magnification. The length-to-width ratio of cells in at least 3 fields of view per experiment (approx. 200 cells per field) was determined in cells exposed to DF and treated with iCRT5 (50 μ M), IWR-1 (10 μ M) or DKK-1 (250 ng.ml⁻¹). The length-to-width ratio of EC exposed to UF are shown for comparison (n=3; analysis by Kruskal-Wallis test with uncorrected Dunn's test). **(C)** HAEC were exposed to flow for 72h and treated with iCRT5 (50 μ M) for the last 24h of flow exposure. HAEC were fixed and stained with ZO-1 and DRAQ5. Mean fluorescence intensity of standardised regions of interest spanning cell junctions was used to quantify ZO-1 expression (n=4; analysis by Mann-Whitney test) **(D)** HAEC were exposed to flow for 72h and treated with iCRT5 (50 μ M) for the last 24h of flow exposure or **(E)** transfected with Frizzled-4 siRNA (siFzd4) and exposed to flow for 48h. RNA was harvested from EC exposed to DF and expression of *TIE2*, α -smooth muscle actin (α -SMA) and *SNAIL* assessed by qRT-PCR using *GAPDH* as a housekeeping gene (n=5-6; analysis by Mann-Whitney test).

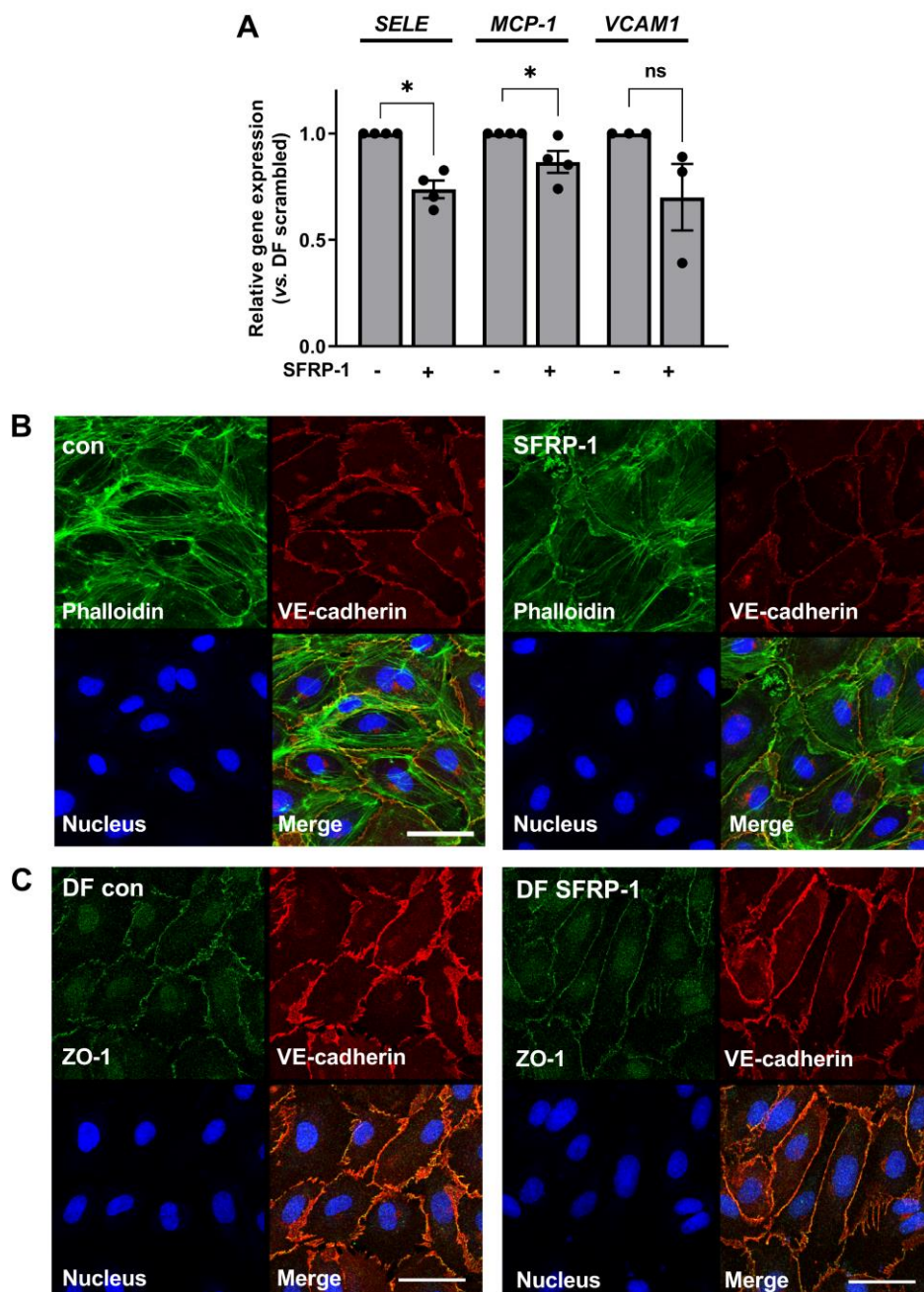


Fig. S6. SFRP-1 reduces inflammatory signalling in EC exposed to disturbed flow and alters cytoskeletal organisation

(A-C) HAEC were exposed to flow for 72h and treated with SFRP-1 (200 ng.ml⁻¹) for the last 24h of flow exposure. **(A)** RNA was harvested from EC exposed to DF and the expression of pro-inflammatory genes assessed by qRT-PCR using GAPDH as a housekeeping gene (n=3-4; analysis by Mann-Whitney test). **(B-C)** EC were fixed and incubated with anti-VE-cadherin antibody, 488-phalloidin or anti-ZO-1 antibody and DRAQ5 nuclear stain (n=4; scale = 50 µm; representative images shown).

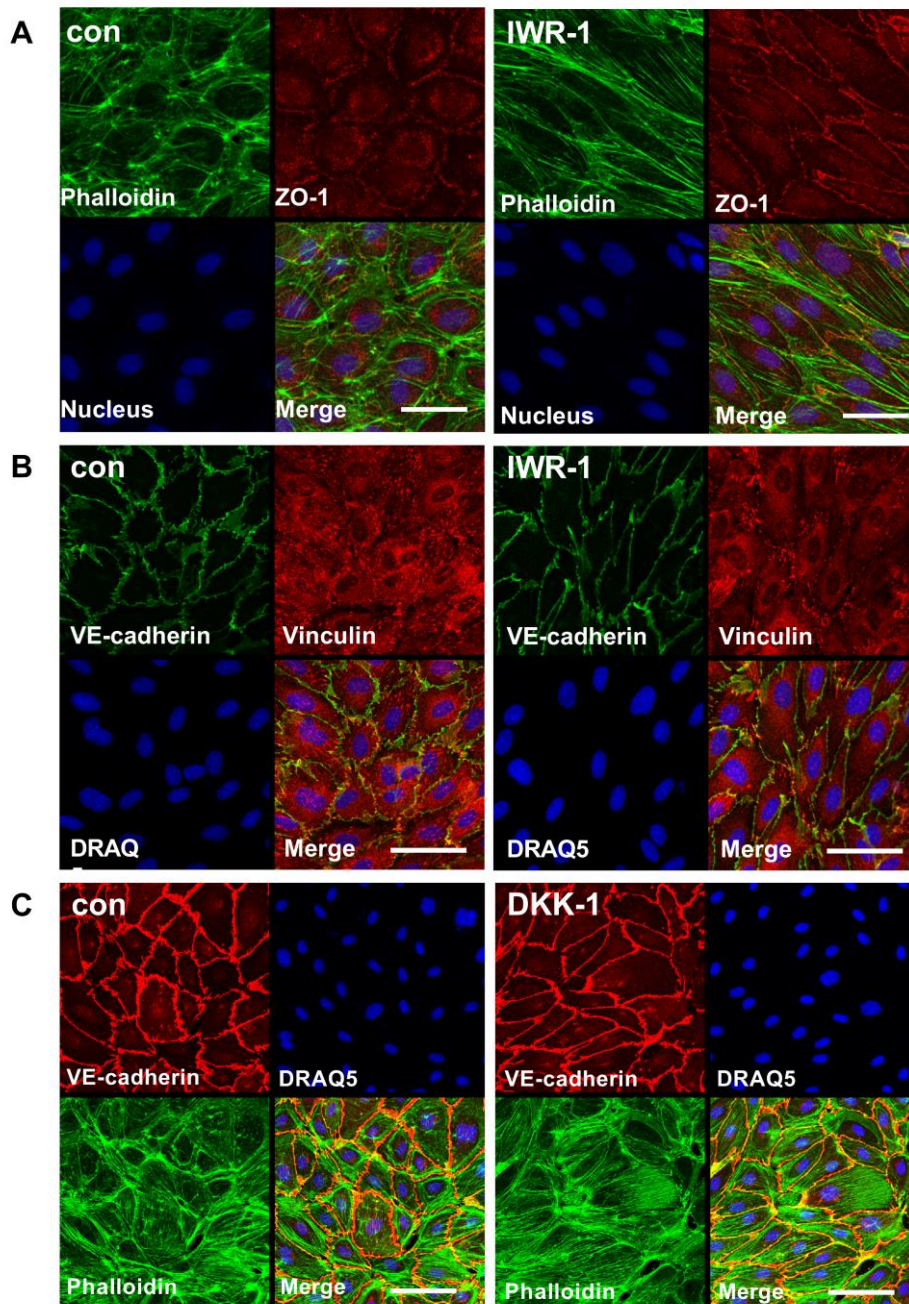


Fig. S7. IWR-1 but not DKK-1 alters cytoskeletal organisation in EC exposed to disturbed flow

(A-C) HAEC were exposed to flow for 72h and treated with (A-B) IWR-1 (10 μ M) or (C) DKK-1 (250 ng.ml⁻¹) for the final 24h of flow exposure. (A-C) EC were fixed and stained with DRAQ5 nuclear stain and (A) 488-Phalloidin and anti-ZO-1 antibody or (B) VE-cadherin and vinculin antibodies or (C) 488-Phalloidin and anti-VE-cadherin antibody. Images obtained from 4 fields of view (n=5; representative images shown; scale = 50 μ m).

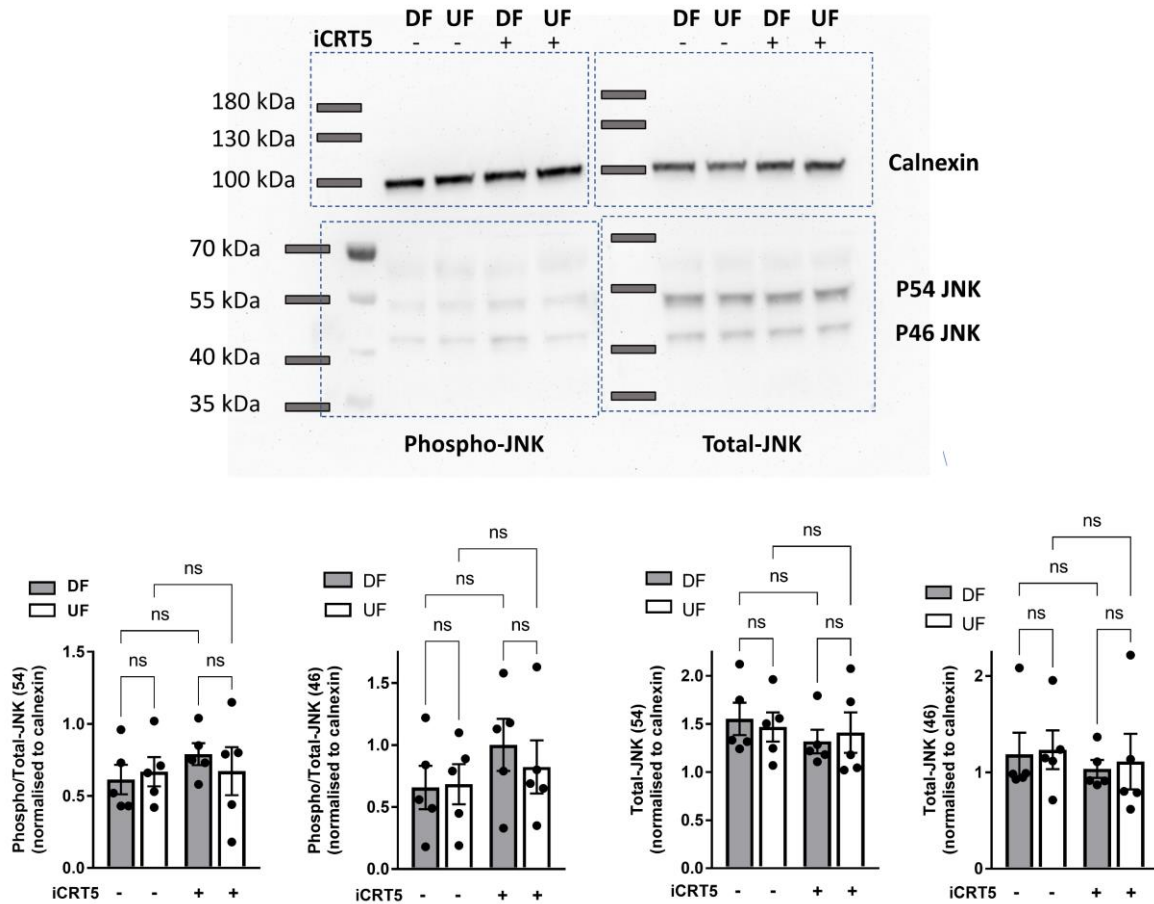


Fig. S8. Expression and phosphorylation of JNK in EC exposed to flow

HAEC were exposed to flow for 72h and treated with iCRT5 (50 μ M) for the last 24h of flow exposure. Lysates from EC exposed to DF and UF were assessed by western blot using phospho-JNK and total JNK antibodies. Calnexin was used as a loading control. Results analysed by one-way ANOVA (n=5; representative blots shown above).

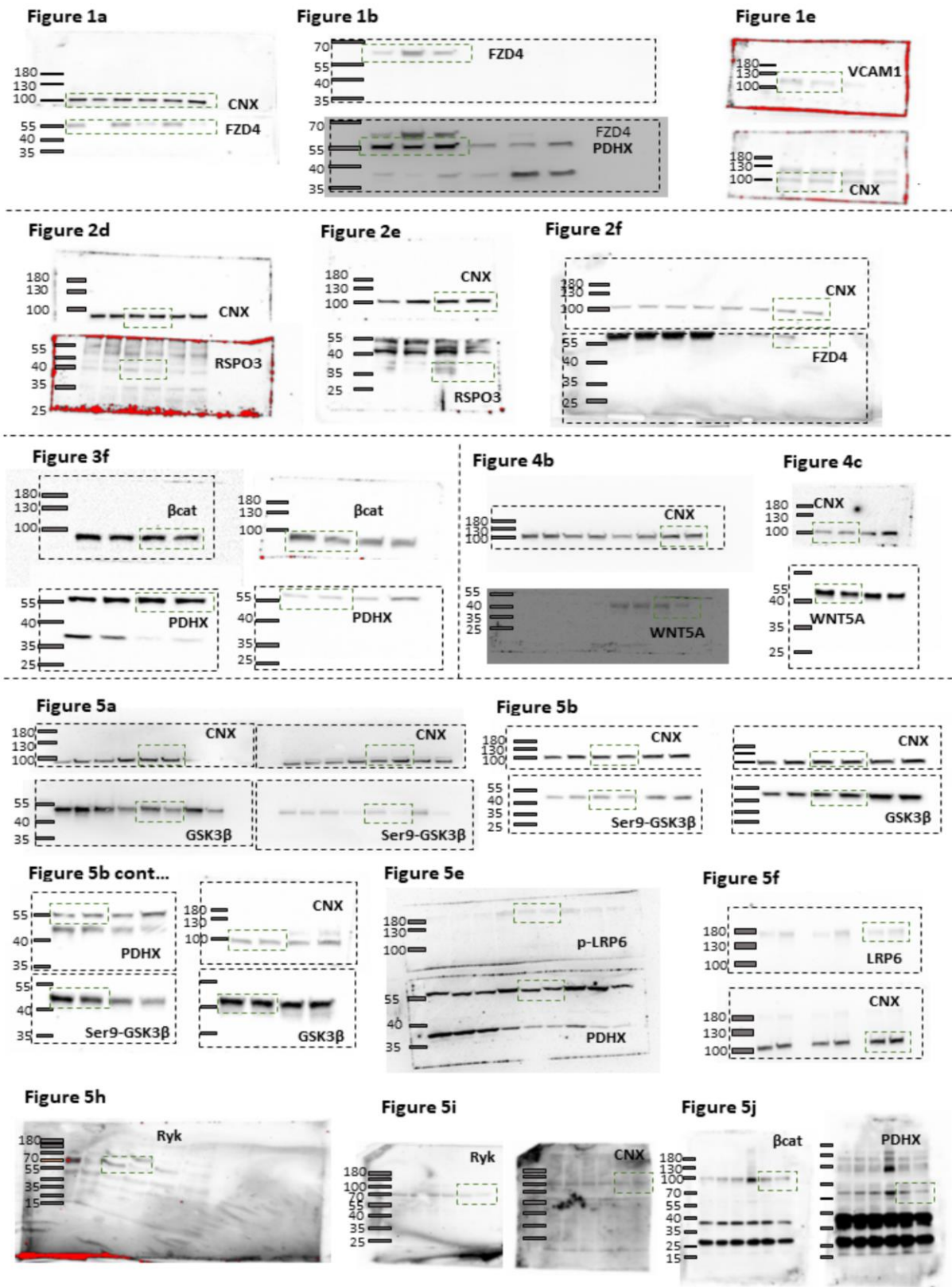


Fig. S9. Uncropped images of western blots used throughout the manuscript. Dotted lines denote bands featured in the relevant figures.

Table S1. Details of antibodies, reagents and cells used

Antibody target	Species	Source	Catalog #	Application	Dilution
β -catenin	Mouse	BD Biosciences	610153	IF	1 in 100
β -catenin	Rabbit	Cell Signaling Technology	9582	WB	1 in 3000
β -catenin (active)	Rabbit	Millipore	05-665	WB	1 in 1000
Calnexin	Goat	Santa Cruz	sc-6465	WB	1 in 3000
Frizzled-4	Goat	Santa Cruz	sc-66450	WB	1 in 1000
Frizzled-4	Rabbit	ThermoFisher	710731	IF	1 in 100
GSK3 β	Rabbit	Cell Signaling Technology	9315	WB	1 in 1000
GSK3 β (Ser9)	Rabbit	Cell Signaling Technology	9322	WB	1 in 1000
JNK	Rabbit	Cell Signaling Technology	9252	WB	1 in 1000
JNK (Thr183/Tyr185)	Rabbit	Cell Signaling Technology	4668	WB	1 in 1000
Lrp6	Rabbit	Cell Signaling Technology	3395	WB	1 in 1000
Lrp6(Ser1490)	Rabbit	Cell Signaling Technology	2568	WB	1 in 1000
PDHX (E3BP)	Mouse	Santa Cruz	sc-377255	WB	1 in 1000
RSPO-3	Rabbit	Proteintech	17193-1-AP	WB	1 in 1000
Ryk	Mouse	R&D Systems	MAB4907	WB	1 in 1000
TBP	Rabbit	Cell Signaling Technology	44059	WB	1 in 2000
VCAM-1	Rabbit	Cell Signaling Technology	13662	WB	1 in 1000
VE-cadherin	Rabbit	Cell Signaling Technology	2500	IF	1 in 500
VE-cadherin	Mouse	BD Biosciences	555661	IF	1 in 500
Vinculin	Mouse	Sigma	V4505	IF	1 in 500
Wnt5a	Rabbit	Proteintech	55184-1-AP	WB	1 in 1000
ZO-1	Rabbit	Cell Signaling Technology	13663	IF	1 in 250

Reagent	Species	Source	Catalog #	Dilution	Vehicle control (v/v)
488-Phalloidin	na	ThermoFisher	A12379	1 in 40	na
DRAQ5	na	Biostatus	DR50200	5 μ M	na
DKK-1	Human	R&D Systems	5439-DK-010	250 ng/ml	PBS (0.1%)
iCRT5	na	Abcam	ab142141	50 μ M	DMSO (0.1%)
MG-132	na	Sigma	M7449	2.5-5 μ M	DMSO (0.1%)
SFRP-1	Human	PeptoTech	120-29	200 ng/ml	PBS (0.1%)
TNF α	Human	R&D Systems	210-TA-020	10ng/ml	PBS (0.1%)

Cell type	Species	Source	Catalog #
Human aortic endothelial cells	Human	Promocell	C-12271
THP-1 monocytes	Human	ATCC	TIB-202

siRNA	Species	Source	Catalog # / ID
β -catenin siRNA (si β cat)	Human	Sigma	Predesigned siRNA ID: SASI_Hs01_00117960
Frizzled-4 siRNA (siFzd4)	Human	Sigma	Predesigned siRNA ID: SASI_Hs01_00241018
RSPO-3 siRNA (siRSPO-3)	Human	Sigma	Predesigned siRNA ID: SASI_Hs01_00012894
Ryk siRNA (siRyk)	Human	Sigma	Predesigned siRNA ID: SASI_Hs01_00047742
scrambled siRNA (scr)	Human	ThermoFisher	Silencer Select Negative Control #4390846
Wnt5a siRNA (siWnt5a)	Human	Sigma	Predesigned siRNA ID: SASI_Hs01_00202618

Table S2. Details of primers used for qRT-PCR

Gene	Forward	Reverse
<i>CTNNB1</i>	TGCCCTGGCTATGTGAGTTT	TCAAATACCCTGCATAGTACGCT
<i>CLAUDIN-5</i>	CCTGTGCCACCGCTTTTTG	CAGCACTGTCTCTCATCCC
<i>ENOS</i>	CATCTTCAGCCCCAAACGGA	AGCGGATTGTAGCCTGGAAC
<i>ESAM</i>	TCACCAACCTTTCGTCTTCCA	CCAGCGTCACATTACATTGGG
<i>E-SEL</i>	GCTCTGCAGCTCGGACAT	GAAAGTCCAGCTACCAAGGGAAT
<i>FZD4</i>	GGATGCTCTGTGGCCTTCT	GGGCATGTGTAGCAGGAAGT
<i>FZD5</i>	GAGAGACGGTTAGGGCTCG	TTCTCAGCGGAGTGACCC
<i>FZD6</i>	GGGAACGGTGGGTTAGACG	CTGGGTCAATTACTCGGGGG
<i>FZD7</i>	GTCGTGTTTCATGATGGTGC	CGCCTCTGTTTCGTCTACCTC
<i>GAPDH</i>	CTATAAATTGAGCCCGCAGCC	ACCAAATCCGTTGACTCCGA
<i>JAM-A</i>	ACGGGAAGACACTGGGACATA	GGATGGAGGCACAAGCAC
<i>JAM-B</i>	AGCAGTAGAGTACCAAGAGGCTA	CTCCGACCCAGTTTCTTCCA
<i>JAM-C</i>	CAAAATTCAGGGAGACTTGCGC	CCTCACAGCGATAAAGGGCT
<i>KLF2</i>	TGGGCATTTTGGGCTACCT	CCCAGTTCCAAGCAACCAGA
<i>MCP-1</i>	AGGTGACTGGGGCATTGAT	GCCTCCAGCATGAAAGTCTC
<i>PECAM-1</i>	CACAGATGAGAACCACGCCT	GGCCCCCAGAAGACAACAT
<i>RNF43</i>	TTGTTTCACCCCGTGGATT	TCACTTGGCATTGCTCTTCC
<i>RSPO1</i>	GCTGGCAAGGACTGGTGTTT	TGGTTGATTGCCTCGACACC
<i>RSPO2</i>	AACCGATGGAGACGCAGTAA	GTTGACATCGGCTACACCCA
<i>RSPO3</i>	GTAGGGGAGAAAGCCACCAC	ACCAGGTTCTCTGAGTTAGCA
<i>RSPO4</i>	CACAATGGAAAGACCTGCGG	GACTCAGAAAGCACCTGGCA
αSMA	CCGGGACTAAGACGGGAATC	TTGTCACACACCAAGGCAGT
<i>SNAIL</i>	CGAGTGGTTCTTCTGCGCTA	TGCAGCTCGCTGTAGTTAGG
<i>TIE2</i>	TCCTTGGCTCTGCTGGAATG	GGTTCTTCCTCACGTTTTGG
<i>VCAM-1</i>	GTCTCCAATCTGAGCAGCAA	TGGGAAAAACAGAAAAGAGGTG
<i>VE-CADHERIN</i>	ATGAGATCGTGGTGGGAAGCG	TGTGTACTTGGTCTGGGTGAAG
<i>ZO-1</i>	GTGGGTAACGCCATCCTCTG	CCATTGCTGTGCTAGTGAGC
<i>ZNRF3</i>	CTGGGTAGGAGTGGTGAAGC	CTTGCCTAGGACAGTGAGGC